

PHYSICAL PROPERTIES OF NEUTRAL GAS IN M31 AND THE GALAXY

ROBERT BRAUN

Netherlands Foundation for Research in Astronomy, Postbus 2, 7990 AA, Dwingeloo, The Netherlands;¹ and
 National Radio Astronomy Observatory,² Socorro, NM 87801

AND

RENÉ A. M. WALTERBOS³

Department of Astronomy, New Mexico State University, Box 30001, Department 4500, Las Cruces, NM 88003

Received 1990 September 19; accepted 1991 August 8

ABSTRACT

Neutral hydrogen (H I) absorption and deduced emission detected along seven lines of sight through the disk of M31 are analyzed in parallel with published data for the Galaxy. It is shown that the brightness temperature of H I emission is coupled to the opacity of the gas. The Galactic relationship shows asymptotic trends at both large and small opacities. A simple yet effective physical model which accounts for this behavior consists of only two independent components: a high-opacity, cool component of fixed mean temperature, and a low-opacity, warm component of fixed mean brightness. The fitted asymptotic values not only provide a good representation of the data but also are consistent with the much more general constraints imposed by the maximum observed brightness of H I emission and the “threshold” effect of finding detectable absorption whenever the emission brightness exceeds about 5 K. The warm component of H I in the Galaxy is responsible for a mean brightness of about 4 K. The limited data at low opacity in M31 are consistent with this value. The cool Galactic component (in the extended solar neighborhood) has a mean temperature of 105 K, while a radial dependence of gas temperature is observed in M31. Cool-component temperatures in M31 appear to vary from about 70 K at radii between 5 and 10 kpc to about 175 K in the outer disk (10–20 kpc). Intrinsic temperature variations by about a factor of 2 around these mean values are implied by the data.

The gas-to-dust ratio is derived from opacity-corrected integrals of H I to the midplane of M31 versus Balmer-decrement-derived extinctions toward H II regions and supernova remnants. A possible gradient of the gas-to-dust ratio is observed with radius. The slope, $-0.039 \pm 0.008 \text{ dex kpc}^{-1}$, is consistent with the abundance gradient. Gas-to-dust ratios comparable to solar neighborhood values are found at radii between about 10 and 15 kpc in M31.

The most plausible mechanism for accounting for a higher cool-component H I temperature in M31 appears to be a lower mean gas pressure by a factor of about 2. By adopting this gas pressure and the component temperatures of the model fit, the physical properties of the neutral gas are estimated. Deduced volume filling factors of the Galactic H I are about 1% and 15%, respectively, for the cool and warm components, while for M31 they are 8% and 30%. The higher filling factors in M31 are coupled with lower gas densities, especially in the cool phase. The large ratio of surface to volume filling factors for both cool and warm H I suggests that these components are distributed predominantly as large sheet- or shell-like structures. The warm H I component is likely to be physically distinct from the cool component and may instead be associated with diffuse ionized gas at large scale heights in the spiral arms.

Subject headings: dust, extinction — galaxies: individual (M31) — ISM: general — radio lines — atomic

1. INTRODUCTION

Studies of the neutral hydrogen (H I) emission from our own and other galaxies have illustrated the morphology and kinematics of this component of the interstellar medium (ISM). They have not in themselves, however, allowed direct estimation of the physical properties of the gas. At best, using the assumption of low optical depth, it has been possible to obtain a lower limit to the actual column density and hence the gas mass. Constraining the properties of the gas has required complementary studies of the deduced line-of-sight emission and the line-of-sight absorption utilizing background continuum sources.

Since the first observation of H I absorption (Hagen, Lilly, & McClain 1955) there have been a number of extensive surveys of absorption due to Galactic H I. Some of the most useful have been the three major surveys carried out with the Arecibo Observatory by Dickey, Salpeter, & Terzian (1978, hereafter DST78), Payne, Salpeter, & Terzian (1982, hereafter PST82), and Colgan, Salpeter, & Terzian (1988, hereafter CST88), which combined moderate resolution and sensitivity in both H I emission and absorption. More recently, there have been a series of interferometric surveys of absorption (e.g., Dickey et al. 1983; Garwood & Dickey 1989) which have been somewhat limited in utility by the absence of emission data of comparable quality. As various authors have correctly pointed out, high angular resolution, such as that obtained with an interferometer, provides greater sensitivity to absorption along lines of sight to compact background sources. However, once the spatial filtering of a “long” baseline interferometer has been

¹ Postal address.

² The National Radio Astronomy Observatory (NRAO) is operated by Associated Universities, Inc., under National Science Foundation Cooperative Agreement AST-8814515.

³ Hubble Fellow.

applied, it becomes difficult to quantify the extent to which H I emission fluctuations have been “resolved out.” What is clearly much more desirable is complete (in terms of spatial frequency sensitivity) imaging of the H I emission and absorption with high resolution. The two components can then be extracted by simultaneously fitting an appropriate surface and a compact source of known position directly to the images at fixed velocities, instead of relying on the rather arbitrary spatial filtering that results from a given interferometer geometry. The quality of the component fit gives an immediate indication of the uncertainties in the primary observables: the line-of-sight brightness temperature, T_B , and the line-of-sight absorption, $(1 - e^{-\tau})$. Further progress in the analysis of H I absorption and emission properties is likely to depend on such fully sampled observations at high resolution.

A crucial aspect of H I absorption properties within the Galaxy seems to have been overlooked in the existing literature. It has often been stated that H I absorption is a relatively rare phenomenon and that the absorption profiles are in general intrinsically narrower than the associated emission profiles. Careful scrutiny of the Galactic data in DST78, PST82, and CST88 indicates instead that detectable H I absorption ($\tau \gtrsim 0.01$) is seen in any direction and at every velocity where the H I emission brightness exceeds about 5 K. The relative line width of the profiles is therefore sensitively dependent on the level at which the measurement is made, as well as on the peak brightness of the emission profile. By measuring the line profiles near this fixed brightness of about 5 K, identical line widths are found. The reason for this confusion over line widths is the fact that the absorption profiles have a great deal more structure than the associated emission profiles. The explanation for this greater degree of structure almost certainly lies in the very different sensitivities of $(1 - e^{-\tau})$ and T_B to a variation of the actual spin temperature of the gas. This can be illustrated by considering the appearance of three consecutive velocity channels in a spectrum corresponding to identical gas column densities per unit velocity, $T_S \tau = 20$, but for which $T_S = 50, 100,$ and 200 K. This leads to values of $(1 - e^{-\tau}) = 0.33, 0.18,$ and 0.095 and values of $T_B = 16.5, 18.1,$ and 19.0 K. A factor of 3.5 variation in the absorption spectrum is accompanied by an almost undetectable variation in emission. Even modest variations in T_S will result in significant structure in the absorption spectrum, while only marginally affecting the emission. This “threshold” condition for H I absorption will play an important role in the discussion which follows.

A growing number of detections of H I absorption in extragalactic systems is now being made. Single lines of sight have been detected toward about 30 galaxies (Dickey 1986 and references therein; van Gorkom et al. 1989 and references therein). Most successful observations to date have utilized a bright nuclear component to achieve sufficient sensitivity in absorption. More comprehensive data for a nearby galaxy would be extremely valuable, from the point of view both of determining the intrinsic properties of another system from a statistically significant sample and of comparing these properties with those of the (solar neighborhood of the) Galaxy. This last qualification arises from the difficulties of interpretation which accompany the long lines of sight at low Galactic latitudes.

We report the detection of H I absorption and deduced emission along seven lines of sight through the disk of M31 using the Very Large Array (VLA) survey of Braun (1990a), with a

total of 53 independent velocity channels containing absorption features at a level \geq of 2σ or above. The integral absorption and total sampled path length are comparable to those obtained in either of the earlier Arecibo surveys quoted above for the Galaxy. The observations and data reduction have already been described in the original reference, so we turn directly to the extraction and presentation of the line-of-sight observables in § 2. In § 3 we embark on a parallel analysis of the published Galactic Arecibo and M31 VLA data. It will be seen that the often-quoted relationship between apparent spin temperature $\langle T_S \rangle$ and opacity τ is not necessarily the most sensitive to the physical properties of the neutral gas. The relationship between the primary observables themselves, τ with the emission brightness T_B , is the most revealing and allows a sensitive comparison with physical models. A discussion of the results and their implications follows in § 4.

2. THE DATA

The results of a sensitive survey of the H I emission from the northeast half of M31 are presented in Braun (1990a). The most important parameters of this survey are the spatial resolution of $10''$ (corresponding to 33 pc at the 690 kpc assumed distance to M31; Baade & Swope 1963), 5.15 km s^{-1} velocity resolution, and uniform sensitivity of 2 mJy beam^{-1} corresponding to 6.6 K over the region from about $-5'$ to $+70'$ along the major axis and $-15'$ to $+15'$ in minor-axis coordinates. Uniform sensitivity over an extended region was obtained with a 10-pointing mosaic on a regular grid. Full sensitivity to all spatial scales between about 1° and $10''$ was realized by utilizing the B, C, and D configurations of the VLA and using a joint deconvolution of the 10 pointings to reconstruct the largest spatial scales. The integral H I emission over the observed region agrees with the value observed with the Effelsberg filled aperture by Cram, Roberts, & Whitehurst (1980) to within 10%.

An accurate knowledge of continuum sources in this region comes from the survey of Braun (1990b). Another 10-pointing mosaic utilizing the B, C, and D configurations of the VLA was used to obtain a uniform sensitivity of about $30 \mu\text{Jy beam}^{-1}$ at $5''$ resolution over the same area. Compact sources with a surface brightness at 1465 MHz greater than about $10 \text{ mJy } (10'' \text{ beam})^{-1}$ were isolated from this survey and convolved to the resolution of the H I survey to obtain accurate source positions, Gaussian fit dimensions, and peak surface brightnesses as they would appear in the H I data base. Since all of these sources were observed in the 610 MHz survey of Bystedt et al. (1984), a small (typically 3%) spectral index correction to the peak brightnesses could be made to bring them into line with the H I frequency, 1420 MHz. Relevant source parameters are listed in Table 1. Subsequently, the fitting task IMFIT within the AIPS package was used to fit an appropriate Gaussian of fixed dimensions and position as well as a uniform background level to localized areas around each source within each velocity channel of the H I data base. In each case a $40'' \times 40''$ (corresponding to 130×130 pc) region centered on the continuum source was used for the purpose of constraining the two-component fit. (The background box was shifted slightly to either side in the case of the two lobes of the compact double source 0041+417A/B.) This dimension was adopted as the smallest practical one given the dimensions of the synthesized H I beam (see Fig. 2 of Braun 1990a for a detailed display of the H I beam).

TABLE 1
BACKGROUND SOURCE PARAMETERS

Source (1)	R.A.(1950.0) (2)	Decl.(1950.0) (3)	X (4)	Y (5)	S_{1465} (mJy) (6)	$\alpha_{21.50}$ (7)	B_{1420} (mJy beam) $^{-1}$ (8)	θ_{1420} (9)	Comment (10)
0038+409	00 ^h 38 ^m 35 ^s .948 ± 0 ^o 013	+40° 54' 15".01 ± 0".15	-14.09	-9.21	17.4 ± 0.3	-0.97 ± 0.03	17.9 ± 0.3	10"	Compact; < 2"
0039+410	00 39 03.848 ± 0.013	+41 02 20.58 ± 0.23	-4.43	-10.03	49.0 ± 2.5	-0.91 ± 0.09	28.1 ± 0.4	15	Radio lobe; hot spot
0039+412	00 39 34.549 ± 0.013	+41 13 00.67 ± 0.15	7.50	-12.00	351.5 ± 1.5	-0.76 ± 0.05	360.0 ± 1.5	10	Compact; < 2"
0040+412	00 40 07.340 ± 0.013	+41 10 08.55 ± 0.15	9.04	-5.37	25.2 ± 0.2	-0.23 ± 0.06	25.4 ± 0.2	10	Compact; < 3"
0041+417A	00 41 13.055 ± 0.013	+41 40 52.49 ± 0.15	40.88	-14.49	55.5 ± 0.9	-0.85 ± 0.06	46.6 ± 0.3	11	Extended; ~4"
0041+417B	00 41 15.422 ± 0.013	+41 40 52.98 ± 0.15	41.16	-14.15	48.6 ± 1.2	-0.85 ± 0.06	35.5 ± 0.4	12	Extended; ~6"
0044+419	00 44 02.538 ± 0.013	+41 52 34.01 ± 0.15	69.61	2.82	135.0 ± 6.8	-0.84 ± 0.08	117.5 ± 0.3	11	Core-halo

The “background-level” component in the fits corresponds to the deduced line-of-sight emission in a velocity channel. Structure in the H I emission on scales comparable to the fitting region gives rise to an increased error contribution which is reflected in the individual values listed in Table 2. The rms fluctuation level for deduced H I emission is in most cases smaller than the nominal 6.6 K rms in a 10" beam because of the many independent image pixels constraining the fit. The “Gaussian-height” component in the fit was normalized by the peak brightness of the continuum source to obtain the line-of-sight absorption, $(1 - e^{-\tau})$. The error in the Gaussian height reflects the effects of confusion as well as the intrinsic

fluctuation level of the data. In the case of some slightly extended sources, this error is somewhat less than the nominal point-source rms. An interesting, if rather specialized, point in this regard is the fact that the noise distribution in aperture synthesis images is normally more “spiky” than the beam. This is a result of an “overweighting” of the long relative to the short spatial frequencies. By fitting the image-plane data with a Gaussian which is comparable to, or even slightly more extended than, the synthesized beam it is possible to recover the higher (by a factor of about 1.3) sensitivity of a “naturally” weighted image. The above considerations of realistic, channel-by-channel error estimation and optimized signal-to-noise

TABLE 2
EMISSION AND ABSORPTION DATA

Source (1)	Velocity (km s ⁻¹) (2)	$1 - e^{-\tau}$ (3)	T_B (K) (4)	$\langle T_S \rangle$ (K) (5)	Radius (kpc) (6)
0038 + 409	-418.3	0.4860 ± 0.2123	40.3 ± 3.6	82.8 ± 36.9	8
	-423.5	0.4972 ± 0.1955	27.7 ± 3.3	55.8 ± 22.9	7
	-428.6	0.3575 ± 0.1732	20.5 ± 3.0	57.2 ± 28.9	6
0039 + 410	-294.9	0.1851 ± 0.0463	18.5 ± 1.6	99.9 ± 26.5	5
	-300.0	0.1388 ± 0.0427	19.8 ± 1.6	142.7 ± 45.5	5
	-305.2	0.1530 ± 0.0356	17.5 ± 1.6	114.3 ± 28.7	5
	-310.3	0.2776 ± 0.0534	16.5 ± 2.0	59.4 ± 13.5	5
	-315.4	0.2135 ± 0.0498	14.5 ± 1.6	68.0 ± 17.6	5
	-320.6	0.1174 ± 0.0463	8.9 ± 1.6	75.9 ± 33.0	5
	-325.7	0.0925 ± 0.0534	10.6 ± 1.6	114.1 ± 68.2	5
	-330.9	0.0996 ± 0.0534	11.2 ± 1.6	112.6 ± 62.6	7
	-336.0	0.1423 ± 0.0498	19.1 ± 2.0	134.5 ± 49.1	8
	-341.2	0.3274 ± 0.0605	26.4 ± 2.0	80.6 ± 16.1	8
	-346.3	0.1673 ± 0.0569	30.7 ± 2.0	183.5 ± 63.6	8
	-356.6	0.1103 ± 0.0569	18.8 ± 1.6	170.5 ± 89.3	12
	-361.7	0.1459 ± 0.0463	25.7 ± 1.6	176.4 ± 57.1	12
	-366.9	0.2100 ± 0.0569	49.5 ± 2.0	235.8 ± 64.6	12
	-372.0	0.3096 ± 0.0747	53.8 ± 2.3	173.7 ± 42.6	12
	-377.2	0.1566 ± 0.0783	36.6 ± 2.3	233.9 ± 118	12
0039 + 412	-264.0	0.0608 ± 0.0064	46.9 ± 1.3	770.3 ± 83.8	12
	-269.1	0.1192 ± 0.0064	61.4 ± 1.6	515.1 ± 30.9	12
	-274.3	0.1900 ± 0.0075	59.1 ± 2.0	310.9 ± 16.1	12
	-279.4	0.3675 ± 0.0139	41.3 ± 3.3	112.2 ± 9.9	16
	-284.6	0.0928 ± 0.0058	38.6 ± 1.3	416.2 ± 29.8	16
	-289.7	0.0300 ± 0.0072	27.1 ± 1.6	902.0 ± 224	16
0040 + 412	-279.4	0.1890 ± 0.0551	10.2 ± 1.6	54.1 ± 18.0	5
	-289.7	0.1929 ± 0.0591	18.1 ± 1.3	94.1 ± 29.6	5
0041 + 417A	-166.1	0.0880 ± 0.0193	16.2 ± 1.3	183.8 ± 43.0	15
	-171.3	0.1481 ± 0.0193	26.1 ± 1.3	176.1 ± 24.6	15
	-176.4	0.0880 ± 0.0429	29.0 ± 2.3	330.1 ± 163	15
	-181.6	0.1309 ± 0.0429	28.0 ± 2.3	214.3 ± 72.4	15
	-186.7	0.1717 ± 0.0300	37.3 ± 2.0	217.2 ± 39.7	15
	-191.9	0.0579 ± 0.0322	36.3 ± 2.0	626.5 ± 350	17
	-197.0	0.1502 ± 0.0300	37.3 ± 2.0	248.2 ± 51.4	19
	-202.2	0.1030 ± 0.0343	31.4 ± 2.0	304.4 ± 103	19
	-207.3	0.1524 ± 0.0258	22.4 ± 1.6	147.3 ± 27.1	19
	-212.5	0.0687 ± 0.0343	15.8 ± 2.0	230.7 ± 119	19
0041 + 417B	-135.2	0.1042 ± 0.0479	12.2 ± 2.0	117.2 ± 57.1	11
	-145.5	0.0873 ± 0.0451	8.6 ± 2.0	98.3 ± 55.6	11
	-155.8	0.1127 ± 0.0366	16.8 ± 1.6	149.4 ± 50.7	15
	-166.1	0.1127 ± 0.0366	23.4 ± 2.3	207.9 ± 70.6	15
	-171.3	0.1634 ± 0.0451	35.6 ± 2.0	218.1 ± 61.4	15
	-176.4	0.2225 ± 0.0676	40.3 ± 2.6	180.9 ± 56.2	15
	-181.6	0.0789 ± 0.0366	37.3 ± 1.6	472.8 ± 221	19
0044 + 419	-32.2	0.1183 ± 0.0128	33.0 ± 2.0	279.0 ± 34.4	14
	-37.3	0.6553 ± 0.0221	76.2 ± 2.6	116.3 ± 5.6	14
	-42.5	0.5634 ± 0.0196	98.7 ± 1.6	175.1 ± 6.8	14
	-47.6	0.2749 ± 0.0170	85.1 ± 2.0	309.7 ± 20.5	14
	-52.8	0.0826 ± 0.0128	43.9 ± 1.6	531.7 ± 84.6	15
	-57.9	0.0613 ± 0.0179	21.4 ± 1.6	350.1 ± 106	17
	-63.1	0.0323 ± 0.0102	18.8 ± 1.3	581.6 ± 188	17
	-68.3	0.0621 ± 0.0162	13.2 ± 1.6	212.5 ± 61.3	17
	-73.4	0.0213 ± 0.0102	4.9 ± 1.0	232.6 ± 121	17

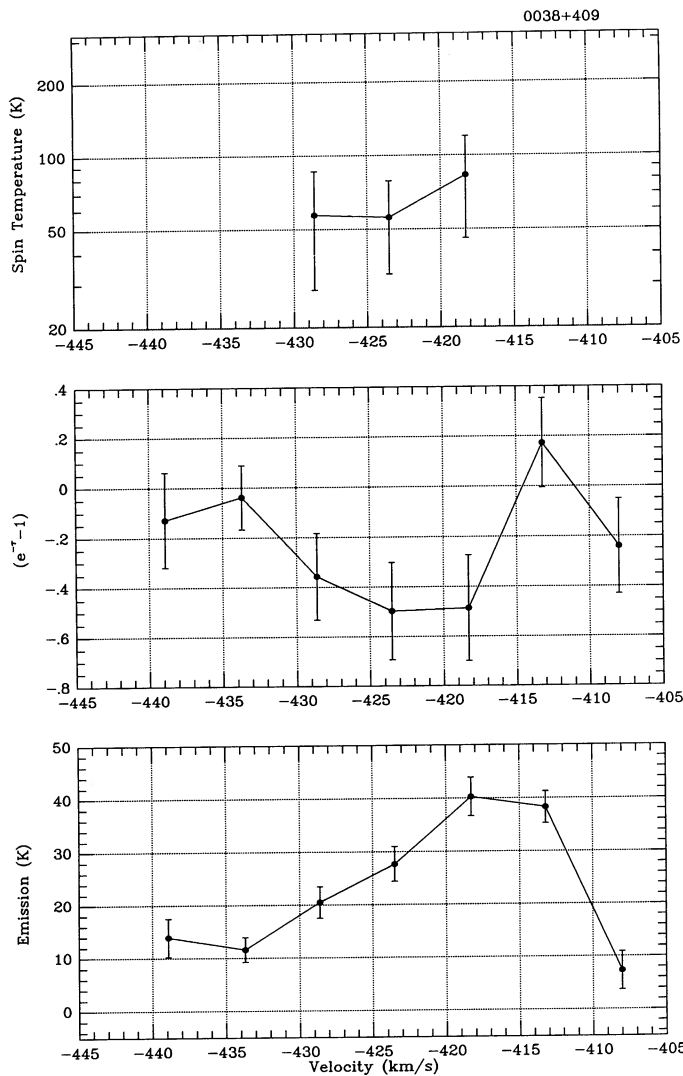


FIG. 1a

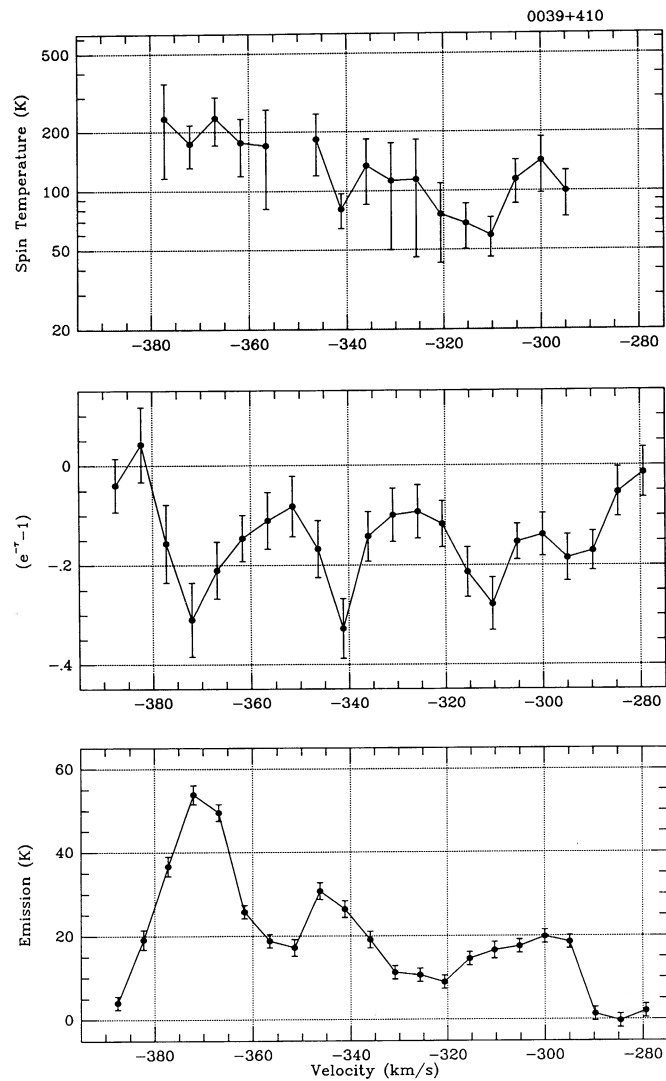


FIG. 1b

FIG. 1.—(a–g) Emission, absorption, and implied mean spin temperature spectra toward the seven background sources listed in Tables 1 and 2. Source names are given at top right. The resolution is 5.15 km s^{-1} in velocity and $10''$ spatially, corresponding to 33 pc in M31. Spectra are derived from a simultaneous fit to the attenuated source and the emission background in a $40'' \times 40''$ ($130 \text{ pc} \times 130 \text{ pc}$) box in the fully (spatial frequency) sampled survey of Braun (1990a).

ratio make it clear why the method of measurement adopted here is superior to the more straightforward practice of simply extracting a spectrum along a single pixel of a data cube.

An important consideration in assessing the quality of the data is the extent to which quantities derived from regions with a radius of 65 pc (the data window used in fitting emission and absorption properties) are likely to be physically relevant. Experience with Galactic emission and absorption studies suggests that severe confusion is encountered in the Galaxy when a data radius larger than about 10 pc is employed. However, a major component of the Galactic confusion is due to our vantage point within the disk of the Galaxy. Even small concentrations of gas can give rise to serious confusion if they are 10–20 times nearer than the actual objects of study along a given line of sight. In external galaxies we have the advantage that all the material along a line of sight is at the “same” distance, so that confusion can only arise from the major gas concentrations themselves. The important question for external galaxies is whether the major gas concentrations are spa-

tially resolved by the data window. In the case of M31, the narrowest emission structures appear to have been well resolved with smallest dimensions of about 100 pc. Experiments with spatial smoothing from 30 to 100 pc linear resolution reveal a *maximum* depression of the brightness of only 15% (Braun 1990a). The linear extent of the data window used in the current study should therefore not unduly undermine its physical relevance.

A related concern in the analysis of Galactic spectra is the spectral confusion which may result from excessively long lines of sight through the Galactic plane. Too many distinct physical regions may overlap within the spectrum to allow an unambiguous association of emission and absorption features. A practical limit of between 5° and 10° latitude seems to be indicated by current work, although some decompositions can be extended down to still smaller latitudes (CST88) along relatively simple lines of sight. The inclination of M31 places it at a fairly constant 13° from edge-on, giving it a favorable orientation from the point of view of spectral confusion.

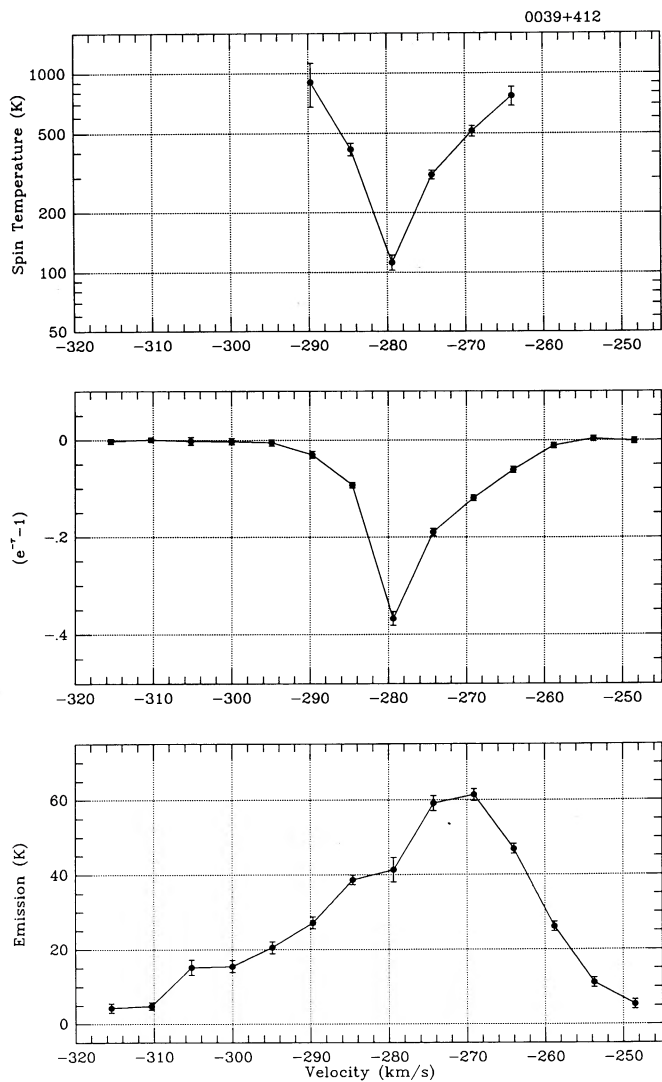


FIG. 1c

The extracted emission and absorption spectra are plotted in Figure 1 together with the implied mean spin temperature, defined by

$$\langle T_S \rangle = \frac{T_B}{1 - e^{-\tau}} \quad (1)$$

at velocities where it is defined at a significance greater than 2σ . These data are also listed in Table 2. Since the velocity resolution is relatively coarse, and is in fact comparable to the FWHM of resolved absorption features in the Galaxy, it is not practical to attempt a decomposition of the spectra into distinct components. Instead we will analyze the independent velocity channels assuming that they represent distinct parcels of gas. Although this is a rather crude assumption, the decompositions of comparable lines of sight in the Galaxy (along latitudes $\sim 10^\circ$) consistently yield an average of one component per 5 km s^{-1} at 5 km s^{-1} intervals wherever $T_B > 10 \text{ K}$ (DST88; PST82; CST88). Equating independent channels in which absorption is detected with individual "components" is therefore not unreasonable. On the other hand, there will likely be an increased scatter in derived quantities, and systematic

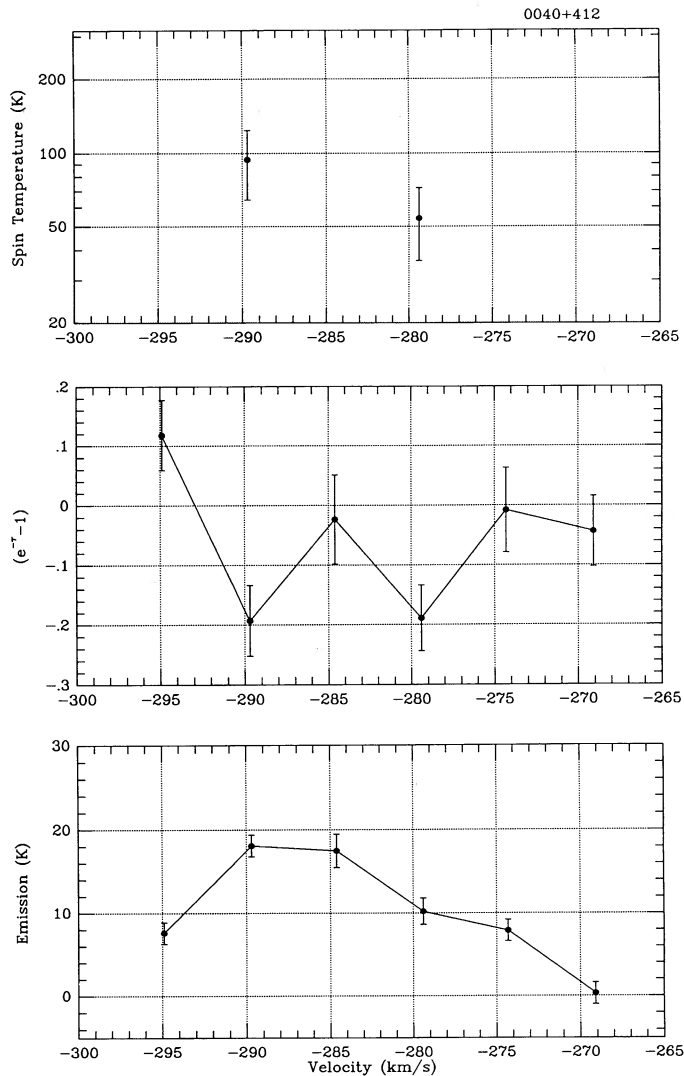


FIG. 1d

errors might arise under some circumstances. If intrinsically narrow lines in emission or absorption have not been fully sampled with the 5 km s^{-1} velocity resolution used here, they will be diluted in frequency and lead to depressed values. In particular, if the absorption were more diluted than the emission, the implied mean spin temperature would be overestimated in such channels, and the spin temperature would be a sensitive function of velocity. This effect only appears to be present near $V = -280 \text{ km s}^{-1}$ in the spectrum toward 0039+412 in Figure 1c, and even here it may well be intrinsic. Implied spin temperatures are in all other cases smooth functions of velocity, so this effect does not appear to be widespread. However, in the extreme circumstance of an unresolved absorption feature occurring in every velocity channel, the mean spin temperatures could be systematically overestimated. The limited sensitivity and resolution of the current data underline the need for caution in their interpretation and the desirability of obtaining independent confirmation.

Notes on the individual sources follow below. Although the detailed correspondence of radii to velocities along lines of sight in M31 is a nontrivial problem, given the highly inclined

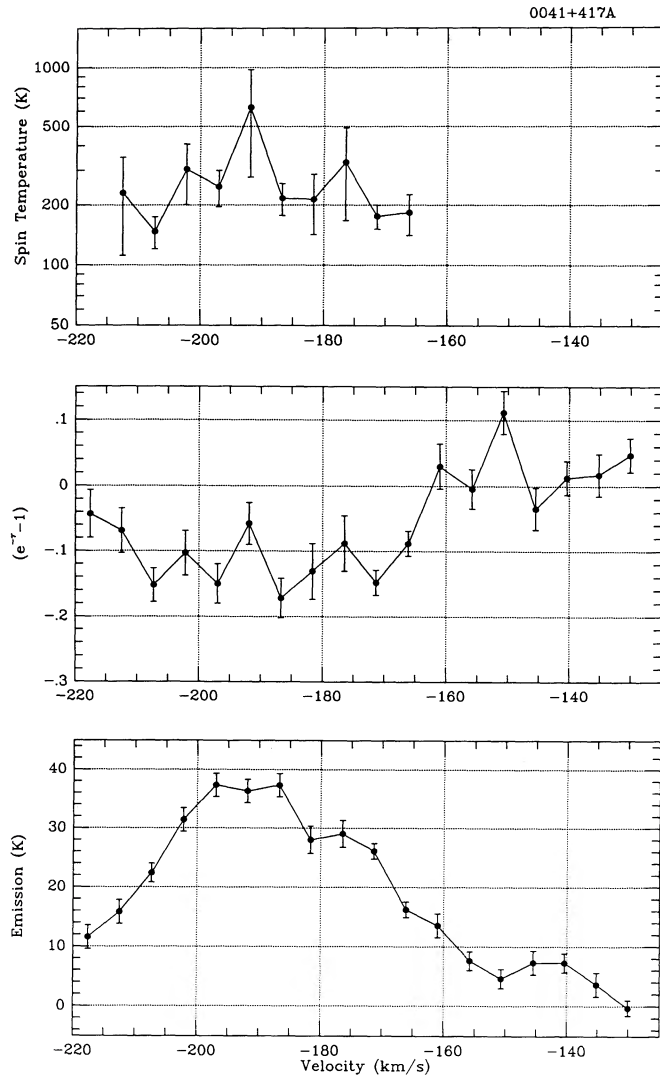


FIG. 1e

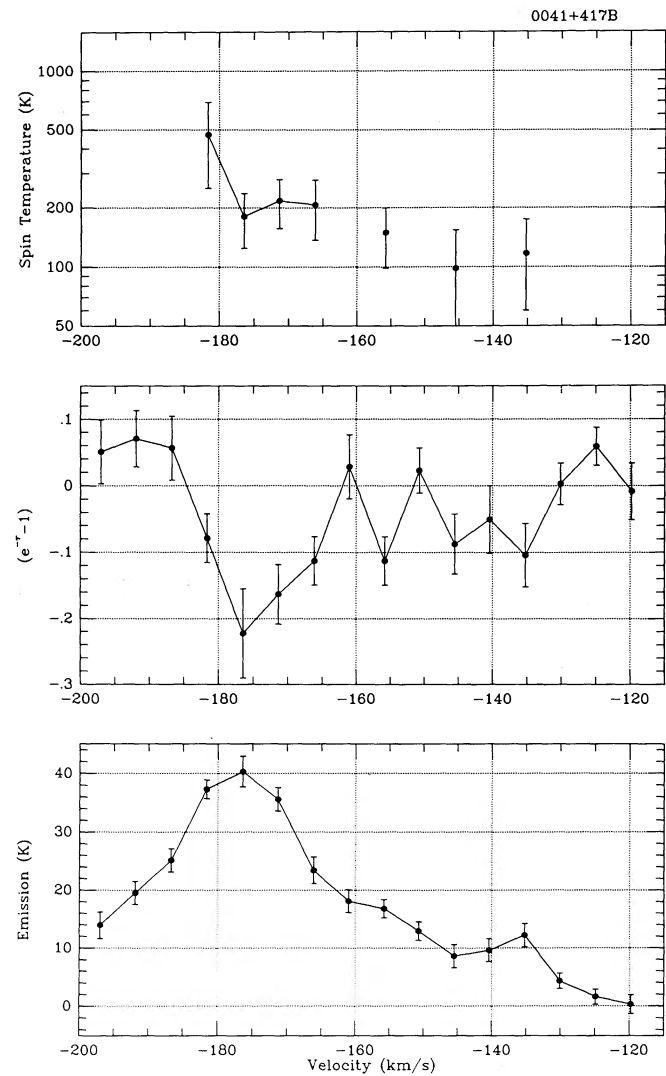


FIG. 1f

nonplanar geometry of the disk (see the kinematic analysis of Braun 1991), it is possible to summarize the global trends very briefly. At major-axis coordinates $|X| > 10'$, velocities most discrepant from the systemic velocity of -315 km s^{-1} correspond to the smallest radii and vice versa. Unfortunately, the situation is less clear near the minor axis, where three of the seven lines of sight are located. Here the distribution and brightness of the extended emission do, however, lead to reasonable identifications of the relevant spiral arm segments. The extended emission in most cases connects the absorbing line of sight to an obvious arm feature in the fixed velocity images of Braun (1990a), while the H I brightness increases smoothly from about 10 K at 3 kpc to in excess of 50 K at 10–12 kpc, and then slowly decreases to 20 K by 20 kpc radius (see Braun 1991).

0038 + 409.—This relatively faint compact source intersects the gaseous disk of M31 near the edge of the coverage of the H I survey and therefore has a relatively high noise level. Modest disk emission is detected between about -367 and -439 km s^{-1} , although the range between -367 and -403 has an even higher noise level because of the staggered velocity

coverage of the original points and is therefore not plotted. The high-brightness H I near -418 km s^{-1} very likely corresponds to the spiral arm at 8 kpc, while the trailing emission to -430 km s^{-1} probably corresponds to the arm at 6 kpc.

0039 + 410.—This bright extended source has an H α nebula from the list of Pellet et al. (1978) near to it in projection, which has led to the suggestion (Dickey & Brinks 1988) that it may lie within M31. Careful examination of the continuum images suggests instead that this is the bright radio lobe of a distant triple radio galaxy with source B29 (from the list of Braun 1990b) being the core and B35 the other radio lobe. Emission is detected at velocities between -295 and -385 km s^{-1} , as well as associated absorption over most of this range. The most likely radii for the three major arm features at -310 , -340 , and -370 km s^{-1} are 5, 8, and 12 kpc, respectively, based on the distribution of the extended emission at these velocities in the channel images of Braun (1990a). The spin temperatures along this line of sight show a clear trend for increasing temperature with radius.

0039 + 412.—This bright, compact source was first detected in absorption by Unwin (1980) and subsequently by Brinks &

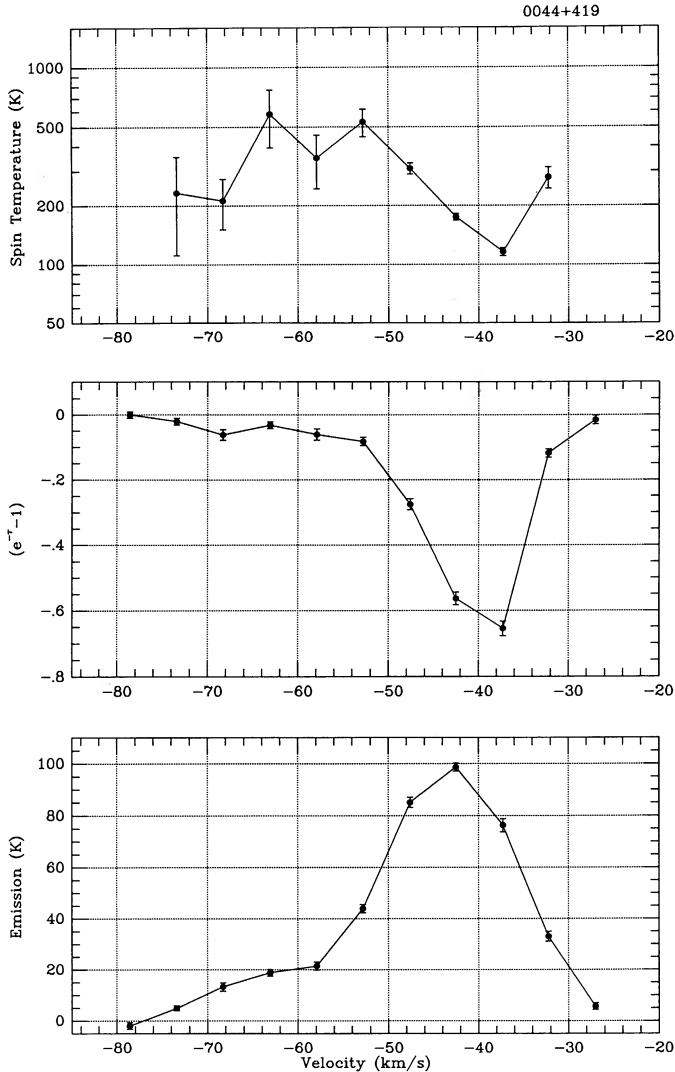


FIG. 1g

Shane (1984) and Dickey & Brinks (1988). The emission spectrum given here differs slightly from that published in Dickey & Brinks (1988) because of the higher spatial and velocity resolution. As stated earlier, the narrow minimum of apparent spin temperature at -280 km s^{-1} may be indicative of an absorption feature which is still unresolved in velocity. This line of sight is confined entirely to the outer galaxy, beyond about 12 kpc. The major emission peak between -265 and -285 km s^{-1} is due to the arms at 12 and 16 kpc, while the fainter emission extending to -305 km s^{-1} with no detectable associated absorption arises in the periphery of the arm at 19 kpc.

0040 + 412.—This relatively faint, compact source is seen in projection against a faint spiral arm in the inner galaxy at only 4.5 kpc radius. Two faint absorption features with a relatively low spin temperature are observed.

0041 + 417A.—This is the brighter, slightly extended component of a double source separated by only $26''$. The $40'' \times 40''$ data window for the fitting of emission and absorption components was shifted in right ascension so as to include only one or the other of these sources at one time. This line of sight contains a faint contribution in emission at -140 km s^{-1}

due to an arm at 11 kpc and more prominent features due to spiral arms at -175 and -200 km s^{-1} corresponding to radii of 15 and 19 kpc, respectively. The implied spin temperatures are relatively constant at about 200 K.

0041 + 417B.—Although only removed by $26''$, this line of sight samples a significantly different gas column than that of 0041 + 417A. This moderately bright, slightly extended source reveals faint absorption in the 11 kpc arm near -140 km s^{-1} . The 15 kpc arm remains prominent, while the 19 kpc arm is no longer prominent in either emission or absorption. Implied spin temperatures increase from about 100 to 200 between 11 and 15 kpc.

0044 + 419.—This bright, slightly extended source is located near the major axis where an arm at a radius of 14 kpc is centered at -45 km s^{-1} . The high-velocity tail extending to -75 km s^{-1} , with implied spin temperatures of about 500 K, corresponds to the outer edges of the 17 kpc arm.

3. ANALYSIS

Before proceeding to an analysis of the observed quantities, it is worthwhile to consider their relation to the physical conditions along a given line of sight. The brightness temperature of H I in emission is

$$T_B(V) = T_1(1 - e^{-\tau_1(V)}) + T_2(1 - e^{-\tau_2(V)})e^{-\tau_1(V)} + T_3(1 - e^{-\tau_3(V)})e^{-\tau_1(V) - \tau_2(V)} + \dots \quad (2)$$

for regions 1, 2, 3, ... of spin temperature T_1, T_2, T_3, \dots at increasing distances along a line of sight. The corresponding absorption is given by

$$1 - e^{-\tau(V)} = 1 - e^{-(\tau_1(V) + \tau_2(V) + \tau_3(V) + \dots)}, \quad (3)$$

since the signal attenuation simply accumulates. The implied mean spin temperature, $\langle T_S \rangle$ is given by the ratio of equations (2) and (3). If each individual opacity as well as their sum is much less than unity, then

$$\langle T_S \rangle = \frac{T_1 \tau_1 + T_2 \tau_2 + T_3 \tau_3 + \dots}{\tau_1 + \tau_2 + \tau_3 + \dots}, \quad (4)$$

i.e., the mean spin temperature is the opacity-weighted mean. Only if all of the individual column densities are also approximately equal will the result be the sometimes quoted harmonic mean. This assumption is so restrictive that it makes the harmonic mean approximation for the spin temperature physically uninteresting in practice.

The actual individual opacities are given by

$$\tau_i = \frac{1.7 n_i s_i}{T_i \Delta V_i} \left[\frac{\text{cm}^{-3} \text{pc}}{\text{K km s}^{-1}} \right] \quad (5)$$

for a hydrogen density n_i , path length s_i , and velocity width ΔV_i . It can be seen from the equations above that if a relatively cool component dominates the total opacity (as might be expected given the inverse dependence on temperature in eqn. [5]), the mean spin temperature will reflect only an upper limit for this component, while the measure absorption will give a reasonable estimate of the associated opacity. On the other hand, if a warm component of low opacity is present, the mean spin temperature gives only a weak lower limit to the actual temperature.

The relationship between the observed and derived parameters, T_B , τ , and $\langle T_S \rangle$, can be presented in various ways to stress

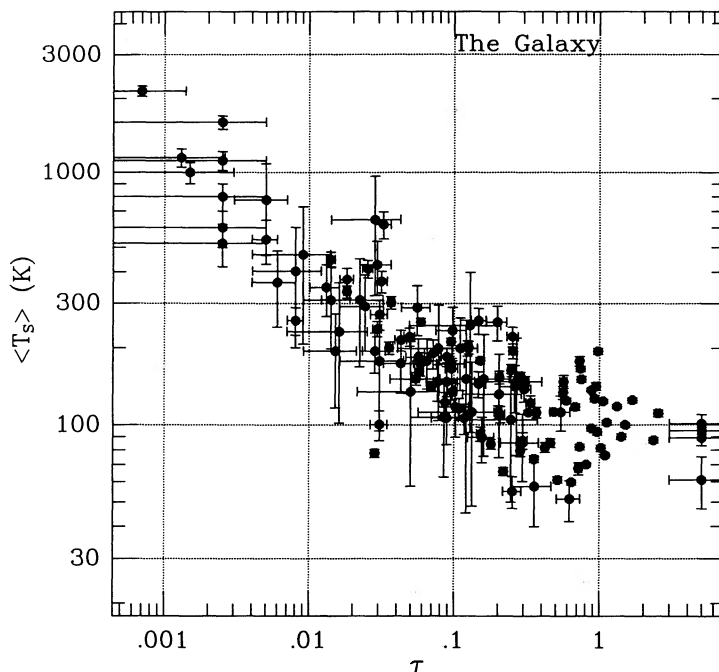


FIG. 2a

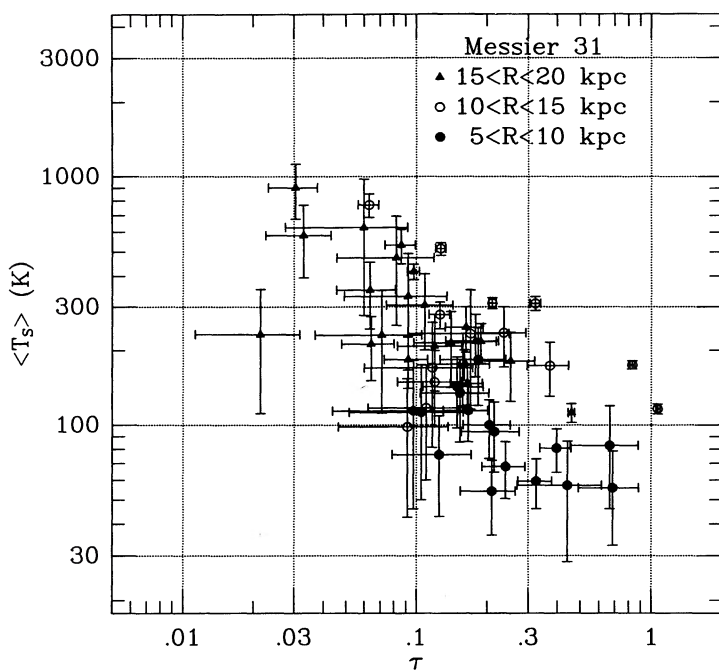


FIG. 2b

FIG. 2.—Implied mean spin temperature vs. measured opacity (a) in the Galaxy from Dickey, Salpeter, & Terzian (1978), Payne, Salpeter, & Terzian (1982), and partially from Colgan, Salpeter, & Terzian (1988) and (b) in M31 from the current work. The values for M31 are binned by radius in that system. Note the systematically cooler implied temperatures of the inner disk relative to the outer disk of M31.

atomic hydrogen. Since Lazareff (1975) first noted a negative correlation between implied spin temperature and optical depth, it has become customary to plot and fit the apparent relationship between these quantities even though they are not independent of one another but are related through equation (1). The fitting has frequently been done in the logarithm rather than in the quantities themselves, so that the resulting fit rep-

resents the lower envelope of the distribution rather than the trend of the arithmetic mean (as pointed out by Kulkarni & Heiles 1988). In Figure 2 the distribution of implied mean spin temperature is plotted against the measured opacity utilizing the data of Table 2 for M31 and the Arecibo data of DST78, PST82, and CST88 for the Galaxy. The high- and intermediate-latitude data of DST78 and PST82 have been supple-

mented by the unambiguous decompositions of CST88 at low Galactic latitude. In practice this has implied using only the CST88 data with $0.5 < (1 - e^{-\tau}) < 0.95$ for the sources 3C 141 through 1923+21 in their Table 2. All double coverages of lines of sight have been edited out of the Galactic data, as well as the apparently anomalously cold feature toward 3C 237. In addition to the Galactic detections, four lower limits to the opacity from CST88 [for which the measured $(1 - e^{-\tau}) > 1$] are plotted as $\tau = 5 \pm 2$ and eight upper limits from the spectra of DST78 and PST82 are plotted as $\tau = 1 \sigma \pm 1 \sigma$. The absence of sources brighter than 300 mJy behind M31 has limited the sensitivity in absorption to opacities greater than about 0.03, so that the low-opacity tail of this distribution could not be sampled. There is clearly a similar, broad distribution with considerable scatter, as has been previously noted for the Galaxy (Crovisier 1981; Payne, Salpeter, & Terzian 1983).

Given the generally ambiguous nature of the "mean" spin temperature noted above, an interpretation does not immediately follow from this combination of parameters. However, at the highest opacities there appears to be a narrowing of the distributions, and in the case of the Galaxy a limiting value of $\langle T_S \rangle \simeq 100$ K seems to be indicated. At the lowest opacities, there is a clear upward trend of "mean" spin temperatures which provides only a weak lower limit of a few thousand kelvins for the warm gas temperature along these lines of sight. Binning the M31 data in Figure 2 by the radius in that system leads to a clear differentiation of the inner and the outer galaxy. The limiting $\langle T_S \rangle$ at high opacity for radii between 5 and 10 kpc is only about 80 K, while for the outer galaxy (10–20 kpc) a limiting temperature about twice as high is indicated. Further differentiation of the intermediate (10–15 kpc) relative to the large (15–20 kpc) radii cannot be construed from the limited quantity of data.

A more obvious relationship to consider is that between the primary observables, T_B and τ . The M31 data of Table 2 and the Galactic data from the references noted above are plotted in Figure 3. This relation is best defined for the Galaxy where the data extend both to lower and higher opacities and the scatter is smaller. The lower scatter is likely due to the fact that the Galactic values are based on decompositions rather than single velocity channel values and also that they apply only to the region within a few kiloparsecs or so of the solar neighborhood rather than lines of sight sampling radii between about 5 and 20 kpc in M31. Indeed, binning the M31 data by radius in Figure 3 reveals the same type of trend noted earlier in relation to Figure 2. The inner galaxy ($R < 10$ kpc) has a systematically lower brightness and higher opacity than the outer galaxy. This trend does not seem to extend to a further differentiation of the intermediate- and high-radius bins, where the primary effect appears to be the greater gas content, and hence higher T_B , in the range $10 \text{ kpc} < R < 15 \text{ kpc}$ than for $R > 15 \text{ kpc}$.

What is suggested by the Galactic data in Figure 3a is that the opacity becomes large as an asymptotic brightness, $T_B = T_\infty$, is approached and that the opacity approaches zero at a small, finite brightness $T_B = T_0$. The features with the highest emission brightnesses are systematically associated with the highest optical depth, while emission brightnesses of less than about 3 K are almost never accompanied by detectable absorption. This second trend is the manifestation of the "threshold" effect which was noted in § 1, and has been generally attributed to an independent, not strongly absorbing (INSA) component of H I in the literature. We will next consider various parameterizations of this relationship.

At intermediate brightnesses and opacities the relation in Figure 3a appears to be roughly linear in $\log \tau$ versus $\log T_B$. A two-parameter power-law fit yields

$$T_B = (60 \pm 7)\tau^{0.60 \pm 0.07} \quad (6)$$

for the Galaxy, which has been overlaid on the data in Figure 4a. Although this functional form provides quite a reasonable description of the intermediate measured values, a physical interpretation is far from obvious. Furthermore, the large predicted values of T_B for large τ are clearly in conflict with experience. Instead, a well-defined upper limit to the brightness of H I in emission is apparent from surveys of Galactic H I. Independent of increased spatial or velocity resolution, peak T_B 's are never observed in excess of about 125 K in the Galaxy (e.g., Schmidt 1957; Burton 1970). In M31 a similar effect is observed, but at a distinct maximum brightness of about 160–180 K (Braun 1990a). Nor does this functional form predict the "threshold" effect noted above. It predicts a continuous association of absorption with emission, rather than the observed tendency to find significant opacities if and only if the emission brightness exceeds some limiting value.

The simplest physical model which might be considered to describe the emission and absorption properties of neutral hydrogen is a single-temperature model in which all the gas has spin temperature $T_S = T_\infty$, which gives,

$$T_B = T_\infty(1 - e^{-\tau}). \quad (7)$$

A number of observational facts already rule out a strictly isothermal gas distribution, namely, the greater degree of structure in absorption versus emission spectra (as described in § 1) and the large line widths and high "mean" spin temperatures associated with low-brightness lines. Even so, it is instructive to consider how successfully the inferred gas properties can be described by such a trivial model. Fitting a single-temperature model to the Galactic data yields $T_\infty = 115 \pm 5$ K, which has been overlaid on the Galactic data (in terms of $\log T_B$ versus $\log \tau$) in Figure 4b. The high-opacity behavior is better illustrated in the linear representation of Figure 5a, where curves at +30 K and -30 K are also plotted. Single-temperature fits to the inner ($5 \text{ kpc} < R < 10 \text{ kpc}$) and outer ($10 \text{ kpc} < R < 20 \text{ kpc}$) disks of M31 yield $T_\infty = 75 \pm 15$ K and $T_\infty = 175 \pm 25$ K, respectively, as illustrated in Figure 5b. Although there is a relatively large intrinsic scatter in the M31 data, there is a clear distinction between the inner and outer disks. It also seems significant that the asymptotic temperatures found in both the Galaxy and M31 are consistent with the highest brightnesses observed directly in H I emission, i.e., about 125 K in the Galaxy and about 180 K in M31. For τ greater than about 0.1 this simple model describes the observed relation rather well. Its shortcomings are apparent at small τ , where it predicts a flattening of $d\tau/dT_B$ for small T_B rather than the observed steepening for $T_B < 20$ K as seen in Figure 4b. Perhaps not surprisingly, it will be necessary to include an additional component of warm, optically thin gas in order to account for the distribution of τ at small T_B .

Let us consider the next simplest model in which a cool component of spin temperature T_c and opacity τ_c has warm regions in front of and behind it at temperature T_w and with negligible opacity $\tau_w/2 \ll 1$. The brightness temperature of emission will be approximately

$$T_B \approx \frac{T_w \tau_w}{2} + T_c(1 - e^{-\tau_c}) + \frac{T_w \tau_w}{2} e^{-\tau_c}, \quad (8)$$

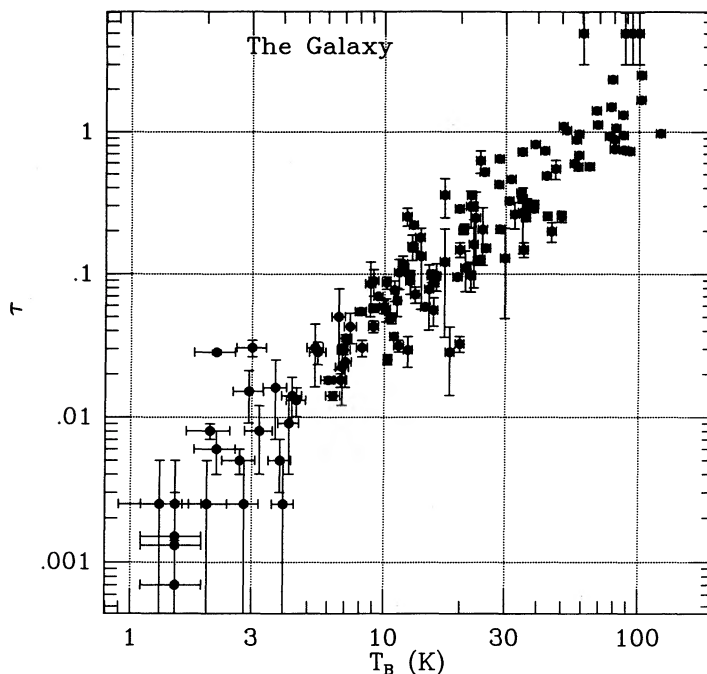


FIG. 3a

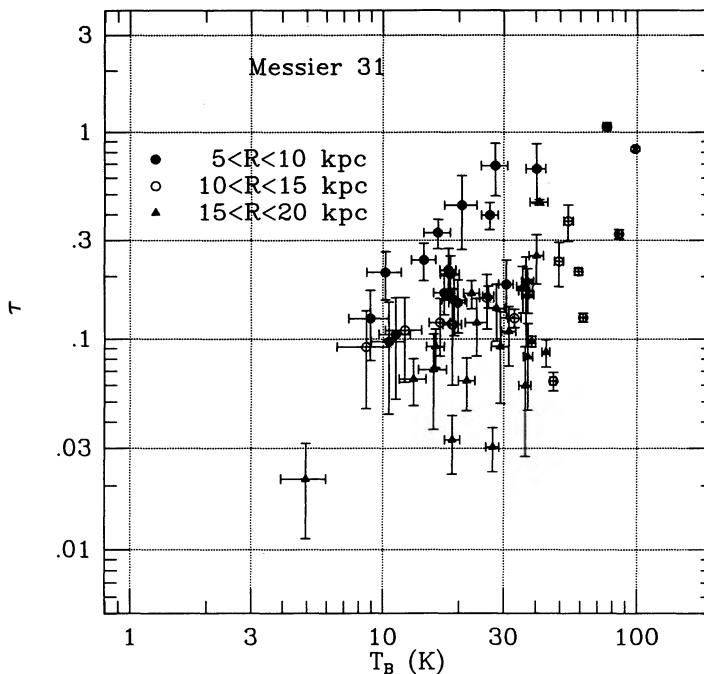


FIG. 3b

FIG. 3.—H I opacity against emission brightness for the Galaxy and M31. (a) Note that the Galactic data extend to both large and small opacities where limiting brightnesses $T(\tau \rightarrow \infty)$ and $T(\tau \rightarrow 0)$ are implied by the extremities of the distribution. (b) The values for M31 are binned by radius in that system and show a systematic displacement of the inner disk to higher opacity at a given emission brightness than the outer disk.

or in terms of the asymptotic brightness (where $\tau_c \rightarrow \infty$), $T_\infty = T_c + T_w \tau_w / 2$, and the limiting brightness (where $\tau_c \rightarrow 0$), $T_0 = T_w \tau_w$,

$$T_B = T_0 e^{-\tau_c} + T_\infty (1 - e^{-\tau_c}), \quad (9)$$

with the two free parameters T_0 and T_∞ . A nonlinear least-squares fit yields $T_0 = 4 \pm 1$ K and $T_\infty = 107 \pm 5$ K for the

Galaxy. Error estimates were obtained from the dispersion in fitted values which resulted from a variety of data-weighting methods in the fitting algorithm (the Levenberg-Marquardt subroutine from Press et al. 1988). The fitted value of T_∞ is not significantly different from that found with the single-temperature fit and is consistent with the previously quoted value of maximum observed H I brightness in the Galaxy.

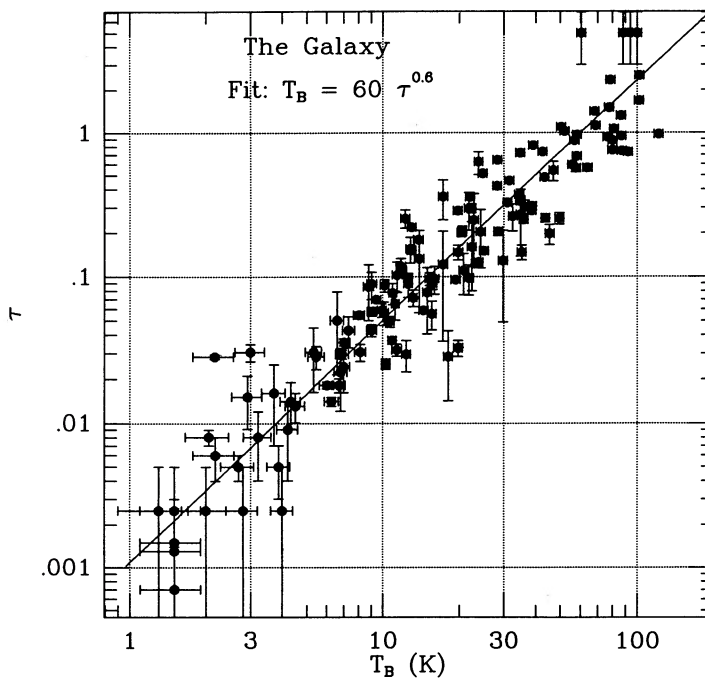


FIG. 4a

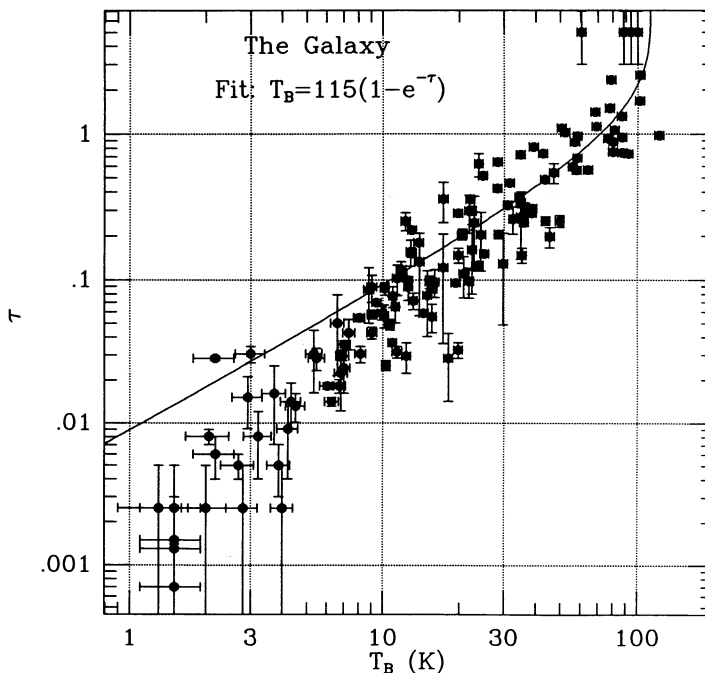


FIG. 4b

FIG. 4.—Parameterizations of the (logarithmic) H I opacity against emission brightness in the Galaxy. (a) The power-law fit of eq. (6) is overlaid on the Galactic data. Although providing a reasonable description of intermediate measured values, this form fails to reproduce the limiting behavior at large and small τ , nor is there an obvious physical interpretation. (b) A single-temperature fit with $T_s = T_\infty = 115$ K is overlaid on the Galactic data. Although such models have an appropriate limiting behavior at large τ , they cannot match the slope of the distribution or its limiting behavior at small τ .

Similarly, the fitted brightness of negligible-opacity, high-temperature gas is consistent with the general result noted in § 1 for the Galaxy, that detectable absorption is observed in all directions and at all velocities where the H I emission brightness exceeds about 5 K. By the time a cool component contributes more than about 1 K to the emission, the corresponding

opacity of about 0.01 becomes detectable. This decomposition yields the representative mean cool-component temperature $T_c = 105 \pm 5$ K in the Galaxy. The functional form for the Galaxy,

$$T_B = (4 \pm 1)e^{-\tau} + (107 \pm 5)(1 - e^{-\tau}), \quad (10)$$

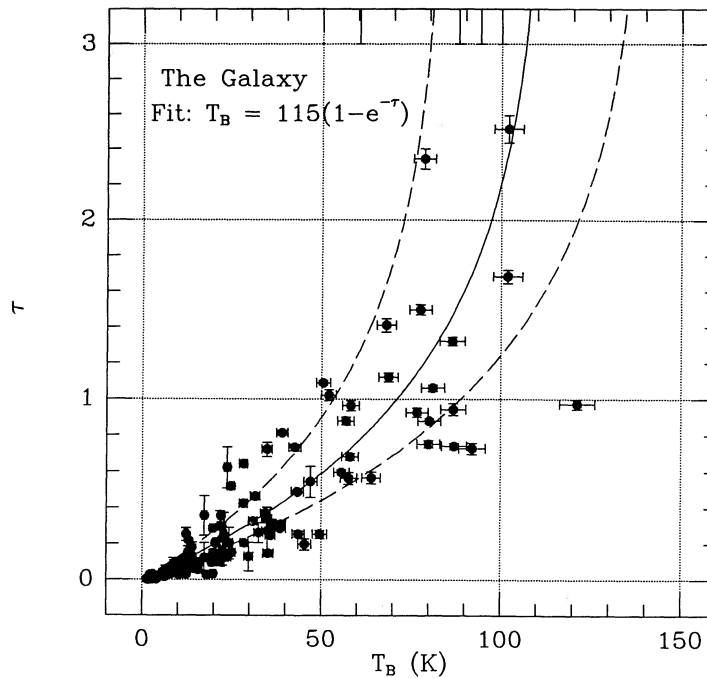


FIG. 5a

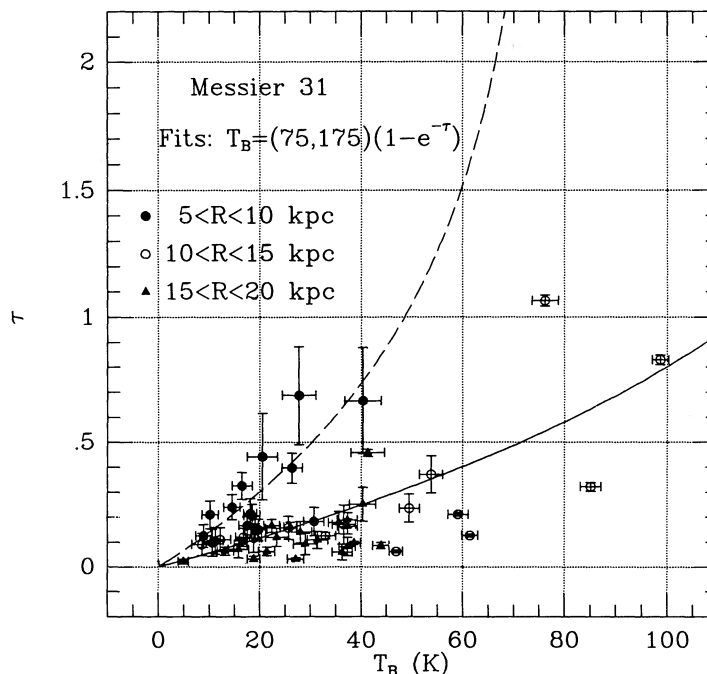


FIG. 5b

FIG. 5.—Parameterizations of the (linear) H I opacity against emission brightness in the Galaxy and M31. (a) A single-temperature fit with $T_0 = T_\infty = 115$ K is overlaid on the Galactic data together with dashed curves at $T_\infty = 85$ and 145 K. The intrinsic scatter of the data suggests roughly a factor of 2 variation in the actual gas temperature. This single-temperature model gives a good characterization of the gas properties at all but the smallest opacities, as illustrated in Fig. 4b. (b) Single-temperature fits to the inner ($5 \text{ kpc} < R < 10 \text{ kpc}$) and outer ($10 \text{ kpc} < R < 20 \text{ kpc}$) disks of M31 are overlaid on the data as a dashed line for $T_\infty = 75$ and a solid line for $T_\infty = 175$ K, respectively. Note the clear distinction between the inner and outer disks.

has been overlaid on the data in Figure 6a, together with curves at $+50\%$ and -50% of the variable values to accommodate the observed scatter [i.e., at $(T_0, T_\infty) = (2, 55)$ and $(6, 160)$]. This degree of intrinsic scatter of the data is consistent with a factor of about 2 variation in both the cool-component temperature and the warm-component column. *Strictly iso-*

thermal components are not consistent with the observed distributions. It seems very striking that such a simple physical model should be so successful in representing the observable properties of neutral hydrogen over two orders of magnitude in emission and four in opacity. Further refinements, such as a scaling of T_0 with Galactic latitude and introducing a depen-

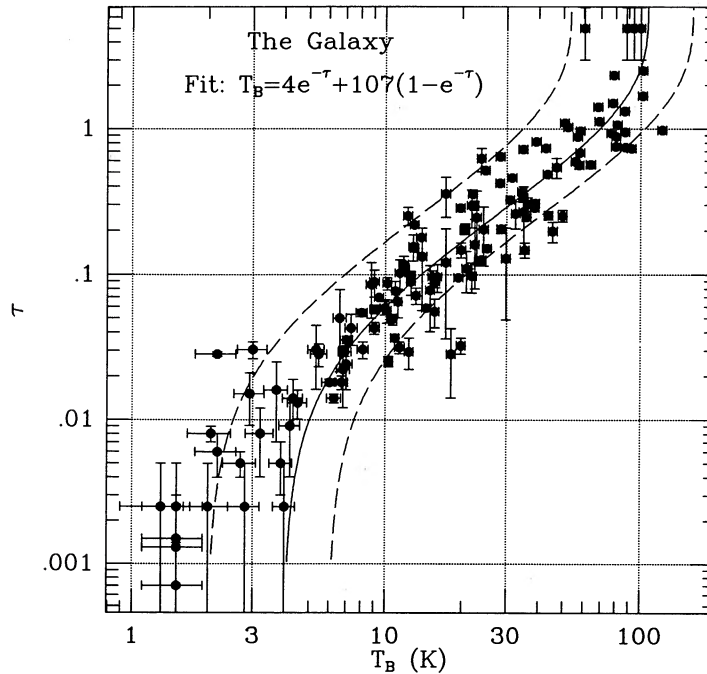


FIG. 6a

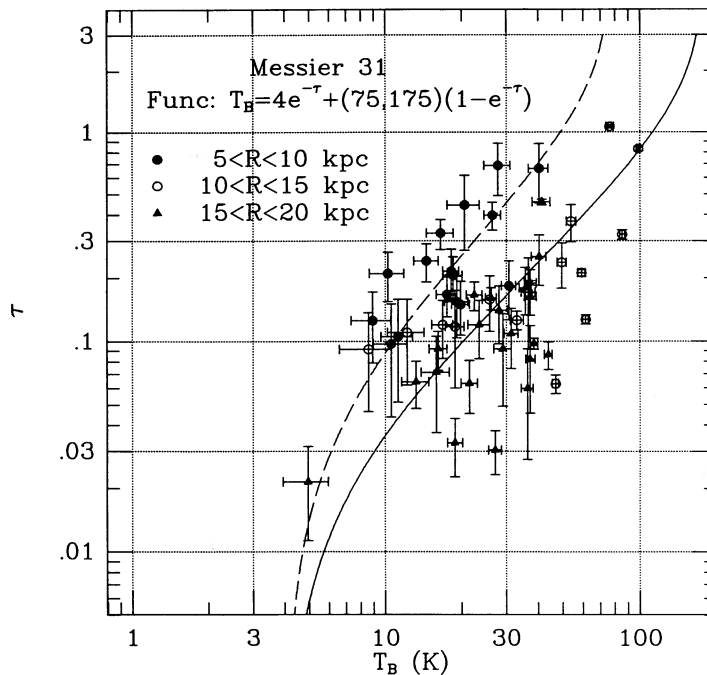


FIG. 6b

FIG. 6.—Parameterization of the (logarithmic) H I opacity against emission brightness in the Galaxy and M31. (a) A two-component model fit as described in § 3 with $T_0 = 4$ K and $T_\infty = 107$ K is overlaid on the Galactic data together with dashed curves at $(T_0, T_\infty) = (2, 55)$ and $(6, 160)$, which form an envelope containing most of the measured points. The fitted value of T_∞ is not significantly different from that obtained in the single-temperature fit. (b) Illustration of a two-component model for M31 using the single-temperature fits for T_∞ to the inner ($5 \text{ kpc} < R < 10 \text{ kpc}$) and outer ($10 \text{ kpc} < R < 20 \text{ kpc}$) disks and the Galactic value of $T_0 = 4$ K. The curves are overlaid as a dashed line and a solid line, respectively.

dence of T_∞ on Galactocentric radius might be fruitful, especially if the data base were extended with high-quality spectra such as may become available with the Green Bank Telescope (GBT).

The current lack of absorption data in M31 at low opacities means that the warm-component column in the two-

component model outlined above is very poorly constrained. For the purpose of illustration, the Galactic value of $T_0 = 4$ K has been combined with the single-temperature fits of $T_\infty = 75$ and 175 K for the inner and outer disks of M31, respectively, and overlaid on the data in Figure 6b. The inner disk, at $5 \text{ kpc} < R < 10 \text{ kpc}$, is quite well described by this form. The

outer disk, at $10 \text{ kpc} < R < 20 \text{ kpc}$, shows considerably more scatter around this parameterization. In particular, some of the gas at the largest radii, $15 \text{ kpc} < R < 20 \text{ kpc}$, seems to indicate either of or both of a higher cool-component temperature and a larger column of warm gas. There are some indications that these tendencies are related to whether arm or interarm gas is being sampled, in the sense that interarm regions may show a higher column due to warm neutral gas. A more detailed physical model which includes the geometry of the spiral arms is likely to give greater insight into the phase content and physical properties of the gas.

A somewhat different approach to explaining the peak brightnesses of H I in M31 and the Galaxy has been given by Dickey (1990). He considers building up a high-brightness line of sight from comparable brightness contributions due to a warm, optically thin foreground component and a cool, optically thick background component using a simplified form of equation (8). By assuming a line-of-sight filling factor of order unity for the intervening warm gas, the warm-gas column can be expressed in terms of the mean free path between cool clouds, and hence the mean opacity, $\langle \kappa \rangle$. With the further assumption that $T_c = 60\text{--}75 \text{ K}$ and the measured Galactic values of $\langle \kappa \rangle = 5 \text{ km s}^{-1} \text{ kpc}^{-1}$, one can derive the necessary density of warm H I, $n_w = 0.2 \text{ cm}^{-3}$, required for total brightnesses of $100\text{--}120 \text{ K}$ as seen in the Galaxy. Quoting the upper limits on the mean opacity in M31 given by Dickey & Brinks (1988) of $2.5 \text{ km s}^{-1} \text{ kpc}^{-1}$, and retaining the same assumptions concerning warm-gas filling factor and cool-gas temperature yields total brightnesses of $160\text{--}180 \text{ K}$. However, the assumptions of small velocity width ($< 26 \text{ km s}^{-1}$) and a low noise level have led Dickey & Brinks (1988) to a very low estimate of the mean opacity in M31. With the higher sensitivity (by a factor ~ 3) and broader spatial coverage (by a factor ~ 6) of the current work, a measured value of $\langle \kappa \rangle = 6.2 \text{ km s}^{-1} \text{ kpc}^{-1}$ is obtained. (The mean opacity follows from the equivalent width of absorption to the midplane divided by the gas scale height, as listed in Table 4.) The argument above would then predict lower peak brightnesses of only $90\text{--}110 \text{ K}$ in M31. Fitting the Galactic data to equation (8) without the assumptions about component filling factor and temperature made in Dickey (1990) leads to rather different results, as has been shown in the preceding paragraphs.

An illuminating analysis of the DST78 and PST82 data has been given previously by Liszt (1983), who considers numerical simulations of neutral hydrogen “cloud” populations which must reproduce a power-law dependence of $\langle T_S \rangle$ versus $(1 - e^{-\tau})$ as well as broader profiles of H I emission relative to absorption features. He considers a cloud-intercloud scenario (with unit filling factor of the intercloud component) and a core-halo cloud model, concluding that a power-law dependence of $\langle T_S \rangle$ versus $(1 - e^{-\tau})$ is easily reproduced with a variety of assumptions, while the two-component isothermal scenarios of the type he considered were insufficient to provide significantly broader emission than absorption profiles. The method of producing intrinsically broader emission profiles that he considers employs the thermal broadening of gas within individual “clouds” at temperatures between 20 and 3000 K. As already discussed in § 1, Galactic absorption profiles measured at a brightness of about 5 K are just as broad as their emission counterparts, so that the demand for differing line widths is not a relevant constraint. The greater complexity of absorption relative to emission profiles does seem to imply at least a modest degree of temperature structure. However,

temperature fluctuations of a factor of about 2 (such as are implied by the scatter about the fit in Fig. 6a) are likely to be sufficient in this respect, rather than the factor of 150 considered by Liszt. By comparing Figures 2 and 3, it also becomes clear that a plot of the mean spin temperature $\langle T_S \rangle$ against opacity τ is not necessarily the most revealing of the gas properties. This tendency is aggravated by plotting $\langle T_S \rangle$ against $(1 - e^{-\tau})$, in which case the high-opacity behavior is completely compressed. In light of these considerations, it is perhaps not surprising that generating a power-law dependence of $\langle T_S \rangle$ versus $(1 - e^{-\tau})$ has not provided a strong constraint on “cloud” or ISM models.

4. DISCUSSION AND CONCLUSIONS

From the preceding section it has become clear that the simplest physical model which can account (very satisfactorily) for the observed relation between H I opacity and emission brightness consists of only two uncoupled components: a cool component which dominates the opacity and gives rise to the asymptotic T_b at high opacity, T_∞ , and a warm component of very low opacity which is present along all lines of sight and leads to the asymptotic T_b at low opacity, T_0 . The relationship is well defined for the Galaxy (and is given by eq. [10]), while a higher mean temperature is indicated for the outer disk of M31. There is significant scatter about the mean Galactic relation which is reasonably well contained within the envelope defined by $+50\%$ and -50% of the variable values, as shown in Figure 6a. This scatter appears to represent intrinsic temperature fluctuations of both the cool component temperature and the warm-component column of about a factor of 2. In the case of M31 a significant component of the scatter seen in Figure 6b is due to radially varying gas properties. In particular, cool-component temperatures appear to be systematically lower in the inner galaxy by about a factor of 2. Comparable radial trends may well be present in the Galaxy, although current high-quality data in both H I absorption and emission are confined to the solar neighborhood.

Although the two-component analysis of the data presented in § 3 may be overly simplistic, and individual numerical values may require refinement as more extensive data become available, it still seems worthwhile to pursue some of the consequences of these admittedly tentative results. We will first consider the consequences of our analysis on opacity corrections for application to H I emission surveys. Next we will attempt to place constraints on some of the conditions which are known to influence the kinetic temperature of H I in the ISM, namely, the gas-to-dust ratio and the gas-phase metal abundance. Finally, we will consider the physical conditions and geometry of the cool and warm neutral gas which are implied by this analysis. At worst, this discussion may stimulate the clever reader to embark on a more physically relevant analysis.

4.1. Opacity Corrections and H I Masses

An immediate consequence of the good single-temperature fits found above is the possibility of expressing the column density of H I, and hence the H I mass, in terms of only the resolved emission brightness and its measured mean asymptotic value, T_∞ (in those cases where circumstances provide at least some lines of sight of high optical depth, $\tau \geq 2$). The column density implied by a given emission brightness is

simply

$$N_{\text{HI}} = -1.823 \times 10^{18} T_{\infty} \Delta V \ln \left(1 - \frac{T_B}{T_{\infty}} \right) \text{ cm}^{-2}, \quad (11)$$

which holds even for significant opacities where T_B approaches T_{∞} . For example, the column due to a brightness of 50 K is underestimated by 18% and 30%, respectively, in M31 and the Galaxy under the assumption of low optical depth. At brightnesses of 100 K the underestimates are 50% and 130%, respectively. The underlying assumption, that both radial and local variations in the gas properties can be neglected, will ultimately limit the validity of this approach. It may, however, be possible to account for at least systematic radial variations under some circumstances.

This result vindicates the "one-component" approach used since the late 1950s (e.g., Schmidt 1957), and most recently by Henderson, Jackson, & Kerr (1982), in determining the H I mass of the Galaxy, since the actual run of opacity can be quite effectively accounted for in this way. The asymptotic temperature, $T_{\infty} = 125$ K, assumed in this reference will lead to a slight underestimate of the gas mass with respect to the value $T_{\infty} = 115 \pm 5$ derived here. On the other hand, the large assumed Galactocentric radius of the Sun is likely to have led to an overestimate of order $(10/8.5)^2 = 1.4$ in their work. The scaled H I mass of Henderson et al. (1982) is about $3.5 \times 10^9 M_{\odot}$. However, uncertainties in the Galactic rotation curve will remain the major stumbling block to obtaining an accurate H I mass for the Galaxy.

Applying the opacity correction of equation (11) to the individual spectra of the resolved H I survey of M31 of Braun (1990a) with $T_{\infty} = 175 \pm 25$ leads to a 19% correction for the integrated column from the northeast half of the galaxy. Together with the integral emission for the entire galaxy from Cram et al. (1980), this leads to an estimated total H I mass of $4.6 \times 10^9 M_{\odot}$. Since the cooler asymptotic temperatures for $R < 10$ kpc have not been taken into account in the opacity correction, the typical brightnesses of 20–30 K will have been undercorrected by about 5% at these radii. This will affect the total gas mass estimate by less than 1%, given the intrinsically low gas content in the inner galaxy. Although the correction on the total mass is relatively modest, individual lines of sight have opacity corrections which exceed a factor of 2. The opacity-corrected column density for the northeast half of M31 is illustrated in Figure 7 (Plate 5). Comparison with the uncorrected emission integral in Figure 4 of Braun (1990a) illustrates the greater degree of structure which becomes apparent via the nonlinear scaling of the spectra with the opacity correction.

4.2. Gas-to-Dust Ratio

With an opacity-corrected H I distribution in hand, it becomes possible to determine the relationship between H I column and extinction by associated dust. A more complete analysis would include tracers of the molecular as well as the neutral gas, but sensitive imaging at high resolution in CO is not yet available for extended regions in M31. Without a direct measure of the molecular gas distribution it will be necessary to assume that the neutral gas is a reasonable tracer of the total gas content. Accurate optical spectrophotometry for H II regions and supernova remnants (SNRs) in M31 is now available for a few tens of sources through the work of Blair, Kirshner, & Chevalier (1982). The Balmer decrement can be used to

calculate a corresponding opacity at a given wavelength, e.g., H α , by assuming the form of the extinction law with wavelength from

$$\tau_{\alpha} = \frac{A_{\alpha}}{A_{\beta} - A_{\alpha}} \ln \left(\frac{F_{\alpha}/j_{\alpha}}{F_{\beta}/j_{\beta}} \right) \quad (12)$$

(e.g., Mathis 1983), where the A_{λ} are extinctions at wavelength λ , the F_{λ} are observed line fluxes, and the j_{λ} are the intrinsic line emissivities. Using the extinction law of Savage & Mathis (1979) and emissivities from Osterbrock (1974) for H II regions and Raymond (1979) for the SNRs yields

$$\text{H II: } \tau_{\alpha} = 2.26 \ln(F_{\alpha}/2.87F_{\beta}), \quad (13a)$$

$$\text{SNR: } \tau_{\alpha} = 2.26 \ln(F_{\alpha}/3.0F_{\beta}), \quad (13b)$$

for H II region electron temperatures near 10^4 K and a wide range of densities and shock velocities. Using the relations $A_{\alpha} = 2.4E_{B-V}$ (also from Savage & Mathis 1979) and $\tau_{\alpha} = A_{\alpha}/1.086$, equation (13) can be put into the form most convenient to the reader.

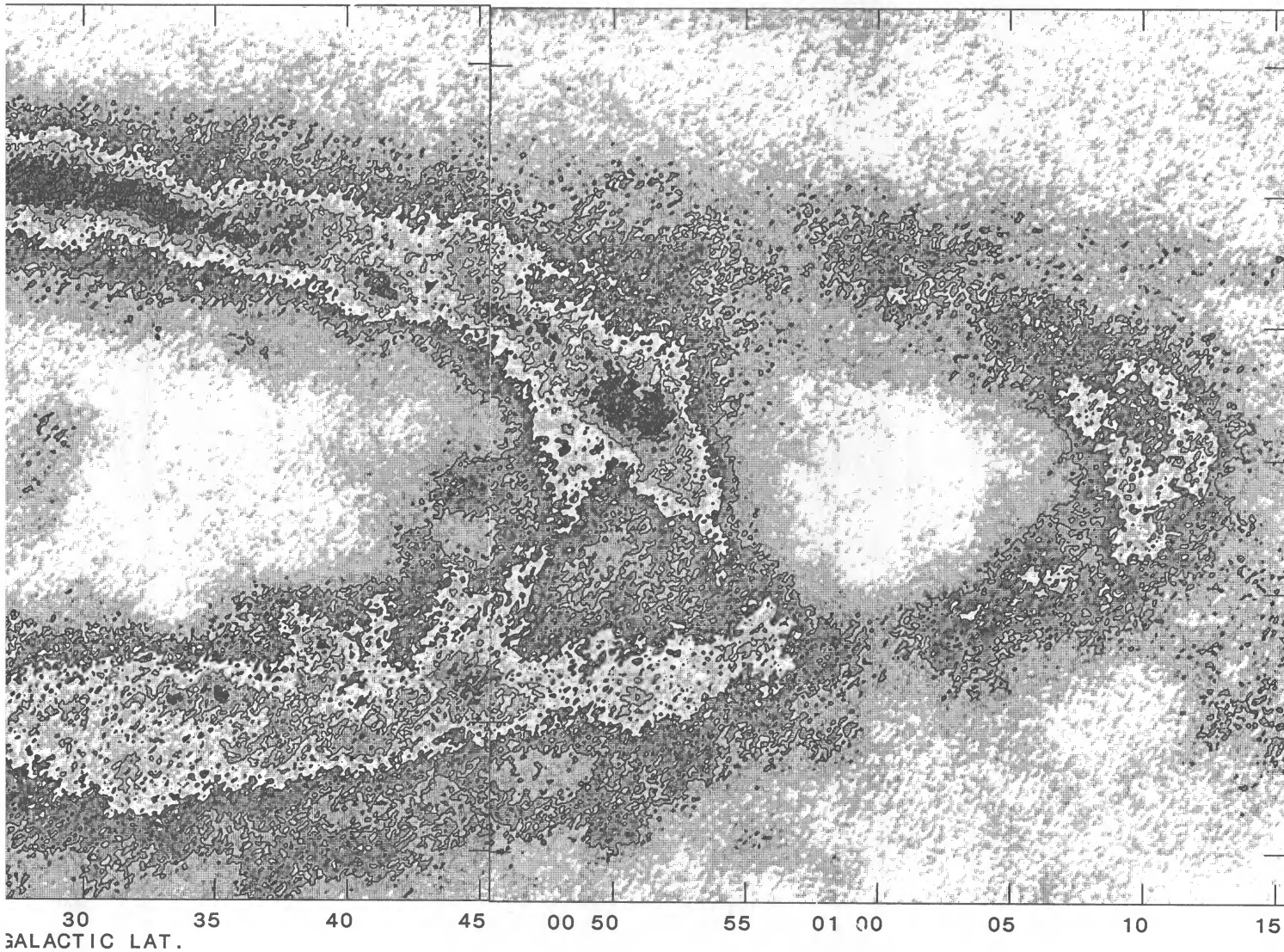
Consistent values of Galactic foreground extinction toward M31 have been determined by a number of authors (Walterbos & Schwing 1987 and references therein), corresponding to $A_B = 0.3$ mag, $E_{B-V} = 0.08$, and $\tau_{\alpha} = 0.18$. Only the residual opacity after correction for the foreground can be expected to be associated with H I within M31.

Although more than 20 regions have been observed by Blair et al. (1982), these lines of sight must satisfy a number of additional criteria to be useful in conjunction with the H I data. The sources must lie in the northeast half of M31 to be contained in the current data base, must have detectable extinction in excess of that due to the Galactic foreground, and must not be unduly confused by multiple peaks in the H I emission spectrum which would lead to ambiguities in the source location and the relevant column. Applying these criteria leaves only the six sources listed in Table 3, of which two have some remaining ambiguity and hence a larger uncertainty. The opacity-corrected H I emission has been integrated over the indicated range of velocity given in columns (4) of the table. All sources were assumed to lie in the local mean plane, so that one-half of the total column was assumed to arise on the near side of the source. Although velocity information in H α is available for some of the sources, it is not yet of sufficient accuracy to provide an improved limit for the velocity integral and so to dispense with the midplane assumption. A 15% uncertainty in the opacities at H α due to uncertainties in the line strengths of H α relative to H β has been assumed.

The resulting values of opacity-corrected H I column per unit optical depth at H α are plotted against radius in Figure 8. The few data points available are suggestive of a trend of

TABLE 3
EXTINCTION CALIBRATION

Source (1)	X (2)	Y (3)	ΔV (km s ⁻¹) (4)	\sum H I/2 (K km s ⁻¹) (5)	τ_{α} (6)	Radius (kpc) (7)
BA 75	16.5	4.3	-63 \rightarrow -434	725 \pm 70	1.42	5.3
BA 22	6.5	12.6	-115 \rightarrow -274	590 \pm 150	0.62	8.7
BA 160	33.1	9.7	-43 \rightarrow -140	980 \pm 140	0.83	9.5
BA 650	65.5	-5.8	-27 \rightarrow -310	1200 \pm 60	0.84	14.3
BA 642	59.2	-6.9	-27 \rightarrow -310	1090 \pm 55	0.92	14.5
BA 581	37.1	-12.2	-156 \rightarrow -310	1230 \pm 80	0.88	15.1



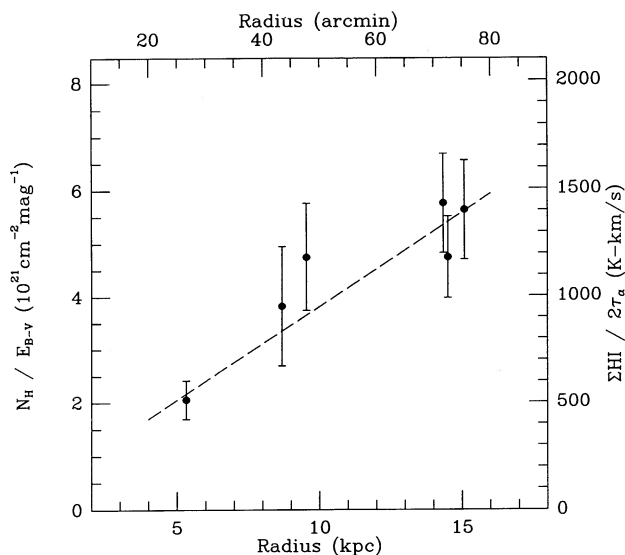


FIG. 8.—Gas-to-dust ratio as function of radius in M31. Opacity-corrected column densities to the midplane are normalized by Balmer-decrement-inferred opacities at $H\alpha$ for $H\ II$ regions and supernova remnants observed by Blair, Kirshner, & Chevalier (1982). The relation is also expressed in terms of $H\ I$ column per unit reddening.

increasing column per unit opacity with radius. A variance-weighted least-squares fit to this distribution yields

$$\sum H\ I / 2\tau_a = (70 \pm 160) + (17.6 \pm 3.3)R\ K\ km\ s^{-1} \quad (14)$$

in terms of the radius R in arcminutes or

$$\frac{N_H}{E_{B-V}} = \left[(0.3 \pm 0.6) + (3.5 \pm 0.7) \frac{R}{10} \right] 10^{21}\ atoms\ cm^{-2}\ mag^{-1} \quad (15)$$

for R in kiloparsecs. Similar values have been reported by Bajaja & Gergely (1977) based on an analysis of integrated $H\ I$ emission toward globular clusters associated with M31. A fit of comparable quality is obtained in $\log(N_H/E_{B-V})$ against R , for which a slope of $-0.039 \pm 0.008\ dex\ kpc^{-1}$ follows. This slope is consistent with that found by Blair & Kirshner (1985) for the abundance gradient for O, N, and S in M31 based on both $H\ II$ regions and SNRs of about $-0.035 \pm 0.01\ dex\ kpc^{-1}$. This consistency suggests that the dust content of the gas in M31 may be directly proportional to the metallicity. This conclusion is, however, sensitive to the assumption that the total gas content is well traced by the neutral gas content. More extensive spectrophotometry or calibrated narrow-band imagery in $H\alpha$ and $H\beta$ could be used to refine the relation in Figure 8 with a potential 50-fold increase in data quantity.

A similar gradient in the dust-to-atomic hydrogen gas ratio has also been found by Walterbos & Kennicutt (1988), although the absolute scaling of the dust-to-gas ratios they found was different. This may be due to the systematic uncertainties associated with the optical measurements of extinction as discussed in that paper as well as the systematic underestimate of $H\ I$ column density by as much as a factor of 2 owing to the absence of opacity corrections to the $H\ I$ data used.

Solar neighborhood estimates of the Galactic reddening due to $H\ I$ are in the range $N_H = (4.8-5.3) < 10^{21} E_{B-V}\ atoms\ cm^{-2}\ mag^{-1}$ (Savage & Mathis 1979 and references therein), corresponding to $\sum H\ I / \tau_a = 1190-1320\ K\ km\ s^{-1}$. Comparable

values, $N_H = (4.4-5.0) \times 10^{21} E_{B-V}\ atoms\ cm^{-2}\ mag^{-1}$, are observed in M31 in the gas-rich region of the disk at radii between about 10 and 20 kpc. The dust content of the outer disk of M31 is clearly very similar to that in the solar neighborhood.

The gas-phase abundance of heavy elements can be assessed by comparing the results of Blair et al. (1982) for M31 with those of Talent & Dufour (1979) for the Galaxy. For convenience and improvement of statistical significance we will employ the generalized “metal” abundance, A , defined by Dopita et al. (1984):

$$\log A = 0.8 + \frac{1}{3} \left[\log \left(\frac{N}{H} \right) + \log \left(\frac{O}{H} \right) + \log \left(\frac{S}{H} \right) \right], \quad (16)$$

which corresponds roughly to $A = O/H$ for typical N/O and S/O . The data for M31 yield $\langle A \rangle = (5.0 \pm 1.0) \times 10^{-4}$ at radii between 10 and 15 kpc with no correction for temperature fluctuations in the $H\ II$ regions, i.e., $t^2 = 0.00$ in the notation of Peimbert (1967). The data for the Galaxy yield $\langle A \rangle = (2.5 \pm 0.5) \times 10^{-4}$ within 1 kpc of the solar neighborhood. The gas-phase coolant abundance is apparently about twice as high over this range of radii in M31 as in the solar neighborhood of the Galaxy.

4.3. Physical Conditions and Geometry

With some knowledge of the temperature and opacity in hand, it becomes possible to constrain the physical conditions and geometry of the $H\ I$ emission structures. The line-of-sight filling factor for a particular component, i , is given by the ratio of internal to total path length, $f_i = s_i/S_i$, or

$$f_i = \frac{T_i^2 \tau_i \Delta V_i}{1.7 p_i S_i} \left[\frac{K^2\ km\ s^{-1}}{cm^{-3}\ K\ pc} \right] \quad (17)$$

by inverting equation (5) for s_i and introducing the thermal pressure p_i in units of $cm^{-3}\ K$. Relevant parameters are listed in Table 4 for both M31 and the Galaxy, in particular the product $\langle T_i \tau_i \Delta V_i \rangle_{\perp}$, which is normalized to a perpendicular line of sight to the midplane. The remaining unknowns in equation (17) are the pressure, the scale height, S_i , and, in the case of the warm $H\ I$, the temperature.

A particularly elegant analysis of the warm ionized medium (WIM or diffuse ionized gas [DIG]) in the Galaxy by Kulkarni & Heiles (1988), based on the different scale heights observed for the volume-averaged electron density, $\langle n_e \rangle$ as determined from pulsar dispersion measures and $\langle n_e^2 \rangle$ as determined from diffuse $H\alpha$ emission, yields simple expressions for the distribution of electron density, volume filling factor, and thermal pressure as a function of out-of-plane height (given in their eqs. [3.28], [3.29], and [3.30]). Specifically, for the gas pressure in the Galaxy they derive

$$p \sim 4000 e^{-|z|/4.28} cm^{-3}\ K. \quad (18)$$

Their result is based on quantities which are as yet poorly defined, since the relatively small scale height of the pulsar distribution only allows a lower limit to be placed on the $\langle n_e \rangle$ scale height, while the $\langle n_e^2 \rangle$ scale height is still based on only a single spiral arm feature. Even so, their result is attractive in its simplicity and consistency with the few other available determinations of the interstellar pressure.

A comparable analysis for M31 has not yet been made, although extensive imaging of the WIM in $H\alpha$ and $[S\ II]$ is now

TABLE 4
GLOBAL PROPERTIES OF NEUTRAL GAS

PROPERTY (1)	SYMBOL (2)	UNIT (3)	MESSIER 31			THE GALAXY ^a		
			Cool (4)	Warm (5)	Reference (6)	Cool (7)	Warm (8)	Reference (9)
Equivalent width to midplane	$\langle \tau \Delta V \rangle_{\perp}$	km s ⁻¹	0.936	...	1	0.706	...	7, 8
Velocity width to midplane (at $T_B > 5$ K)	$\langle \Delta V \rangle_{\perp}$	km s ⁻¹	...	6.62	1	...	7.03	7, 8
Brightness temperature	$\langle T \tau \rangle$	K	...	4:	1	...	4 ± 1	1
Temperature	$\langle T \rangle$	K	175 ± 25	8000:	1, 2	105 ± 6	8000:	1, 2
Column to midplane	$\langle T \tau \Delta V \rangle_{\perp}$	K km s ⁻¹	165 ± 25	25:	1	74 ± 5	28 ± 7	1
Scale height	S	pc	150:	400:	1, 3	150	400	2
Thermal pressure	$\langle p \rangle$	cm ⁻³ K	1500:	1000:	1	2960:	2070:	2
Density	$\langle n \rangle$	cm ⁻³	9:	0.13:	1	28:	0.26:	1
Line-of-sight filling factor	$\langle f \rangle$	%	8:	30:	1	1:	15:	1
Opacity-corrected H I mass	M_{HI}	10 ⁹ M _⊙	4.6		1, 4	3.5		1, 9
Gas-to-dust ratio	$N_{\text{H}}/E_{\text{B}-\text{V}}$	10 ²¹ cm ⁻² mag ⁻¹	4.4 – 5.6		1	4.8 – 5.3		10
Gas-phase “metallicity”	$\langle A \rangle$	[O/H] × 10 ⁻⁴	5.10 ± 1.0		5, 6	2.5 ± 0.5		6, 11

^a Galactic values refer to the extended (1 kpc) solar neighborhood.

REFERENCES.—(1) This work; (2) Kulkarni & Heiles 1988; (3) Braun 1991; (4) Cram et al. 1980; (5) Blair et al. 1982; (6) Dopita et al. 1984; (7) Dickey et al. 1978; (8) Payne et al. 1982; (9) Henderson et al. 1982; (10) Savage & Mathis 1979; (11) Talent & Dufour 1979.

being analyzed (Walterbos & Braun 1989, 1991). The measurement of an $\langle n_e \rangle$ scale height is likely to remain considerably more elusive, however.

The cool and warm H I components in the Galaxy appear to be distributed as a Gaussian of about 150 pc and an exponential of about 400 pc scale height, respectively (e.g., Kulkarni & Heiles 1988; Lockman, Hobbs, & Shull 1986). Although there have been efforts to subdivide the neutral medium further, it is not yet clear that the data warrant decomposition into any additional components. The combined distribution of warm and cool H I in M31 appears to be consistent with an exponential with scale height that increases linearly with radius (Braun 1991) to a value of about 400 pc by 15 kpc. Decomposing the distribution into cool and warm components is considerably more difficult in a system like M31, which is removed by more than 10° from edge-on. As a working hypothesis we will assume a Gaussian and exponential distribution like that of the Galaxy, although these distributions may be significantly broader in M31.

The temperature of the warm neutral component is a quantity that is only weakly constrained by the lower limits of a few times 10³ K obtained from the mean spin temperatures observed at low opacities. An upper limit of about 10⁴ K is implied by the mean velocity dispersion of about 9 km s⁻¹ (e.g., Mebold 1972) seen in the Galaxy for such gas. Calculations of the steady state temperatures of H I by Draine (1978) suggest that a stable, 90%–30% neutral component at 8000–10,000 K can be expected for a very wide range of physical conditions. The most promising hypothesis would seem to be that the warm neutral medium (WNM) is in fact this stable component at about 8000 K.

The cool-component temperatures of H I in the outer disk of M31 are significantly higher than those of the Galaxy. The calculations of Draine (1978) quoted above suggest that stable, cool-component H I temperatures in the range of some tens to a few hundred K can be expected, depending on a variety of factors. Holding all other factors fixed, an increased dust-to-gas ratio leads to an increased temperature, an increased gas-phase abundance leads to lower temperature, an increased ionization rate leads to higher temperature, and an increased gas

pressure leads to a lower temperature. As shown in § 4.2, the dust-to-gas ratio of M31 and the Galaxy agree to within 10% at the relevant radii, so this is unlikely to lead to a significant temperature difference. On the other hand, the factor of 2 higher gas-phase heavy-element abundance in M31 is expected to lead to an estimated 10% lower gas temperature. Given the lower star formation rate in M31 than in the Galaxy (Walterbos & Schwing 1987) and the lower radio continuum power, 6.8×10^{20} W Hz⁻¹ at 408 MHz (Beck & Gräve 1982) compared with 6.3×10^{21} W Hz⁻¹ (Beuerman, Kanbach, & Berkhuijsen 1985, scaled to a solar distance of 8.5 kpc), it seems likely that the ionization rate due to both cosmic rays and soft X-rays is also lower in M31. In the absence of quantitative estimates of these ionization rates, we will only remark that this should also lead to a lower gas temperature. The most plausible mechanism which remains to account for the higher cool-phase temperatures in M31, under the assumption of global steady state conditions, appears to be a lower mean gas pressure. The relatively short time scales (<10⁶ yr) for approaching the steady state solutions (Draine 1978) suggest that only a relatively small fraction of a galactic ISM should be participating in strongly time-dependent behavior, especially when the star formation rate is relatively low. On the other hand, local variations in all of the conditions above will lead to a range of observed temperatures as reflected in the scatter seen in Figure 6. The suggestion that the peak brightness of H I emission seen in M31 reflected local pressure variations was first made by Braun & Walterbos (1989), who noted the striking anticorrelation of high-brightness H I with regions of active star formation as traced by H α emission.

Explaining the different mean cool-component temperatures in M31 versus the Galaxy in terms of a different mean gas pressure leads to an estimated factor of 2 lower gas pressure in M31 (compare Fig. 7 of Draine 1978). Integrating the pressure distribution of equation (18) over the appropriate scale heights of the cool and warm H I (as assumed) in M31 and (measured for) the Galaxy leads to the representative pressures in Table 4. The global properties of the neutral gas are then completely specified, with volume filling factors following from equation (17).

The Galaxy appears to be typified by about 1% by volume of cool H I and 15% of warm H I. Surface filling factors for both these components approach unity for lines of sight containing H I emission in excess of 5 K (compare Fig. 6). The high ratio of surface to volume filling factors gives a strong constraint on the geometry of the H I structures. These structures must be predominantly distributed as sheets or shells in order to achieve sufficiently large aspect ratios. Such a geometry is in excellent agreement with the observed highly filamentary and shell-like projected distribution (e.g., Colomb, Poppel, & Heiles 1980). Furthermore, the fixed warm-component column seems suggestive of a truly independent distribution, rather than any form of core-halo structure associated with the cool gas. This is further supported by the very different scale heights of the warm and cool components seen in the Galaxy. In fact, the scale height and likely temperature of the warm component suggest an origin more closely related, or even identical, to that of the DIG.

The lower implied gas pressures in M31, together with the other quantities in Table 4, lead to volume filling factors of 8% and 30% for the cool and warm H I components within the spiral arms. Together, these components appear to fill an almost 3 times larger fractional volume of the ISM in M31 than they do in the Galaxy. This larger filling factor is coupled with a lower mean gas density by about a factor of 3 for the cool H I. Such a low mean density within the condensed H I component may be responsible for a higher threshold against molecular gas condensation, and subsequently star formation.

Refinements to the theoretical analysis of heating and cooling of interstellar gas are long overdue. Lepp & Dalgarno (1988) have discussed some aspects of the problem, but stop short of a comprehensive analysis. The present work suggests

that even steady state solutions may offer a reasonable description of the gas phases. Although further exploration of time-dependent behavior is clearly important, the most pressing need is for a conveniently parameterized system of steady state solutions incorporating our current physical knowledge.

At the same time, there is clearly room for refinement of the observational parameters. Improved statistics could be obtained for M31 by extending the current study to include the southwest half of the galaxy and by pushing to higher sensitivity with a significantly upgraded VLA. Better calibration of the gas-to-dust ratio determination depends only on a program of more extensive spectrophotometry, preferably along or near the major axis to minimize confusion in H I. Extension of such study to other nearby galaxies is an obvious direction worth pursuing. The greatest potential for detailed study is offered by the Magellanic Clouds and M33, followed by the Sculptor, M81, and M101 groups. The point is that the study of ISM physics in extragalactic systems is now within reach, and it offers the potential for a more comprehensive understanding than is likely to be possible from our vantage point for the Galaxy.

The exceptionally critical reading of earlier versions of this manuscript by John Dickey, Elias Brinks, Jay Lockman, and an anonymous referee is gratefully acknowledged. R. W. acknowledges partial support for this work by NASA through grant HF-1010.01-90A awarded by the Space Telescope Science Institute, which is operated by the Association of Universities for Research in Astronomy, Inc., for NASA under contract NAS 5-26555. R. W. wishes to acknowledge the Astronomy Department of the University of California for computer support and for their hospitality.

REFERENCES

- Baade, W., & Swope, H. H. 1963, *AJ*, 68, 435
 Bajaja, E., & Gergely, T. E. 1977, *A&A*, 61, 229
 Beck, R., & Gräve, R. 1982, *A&A*, 105, 192
 Beuerman, K., Kanbach, G., & Berkhuijsen, E. M. 1985, *A&A*, 153, 17
 Blair, W. P., & Kirshner, R. P. 1985, *ApJ*, 289, 582
 Blair, W. P., Kirshner, R. P., & Chevalier, R. A. 1982, *ApJ*, 254, 50
 Braun, R. 1990a, *ApJS*, 72, 755
 ———. 1990b, *ApJS*, 72, 761
 ———. 1991, *ApJ*, 372, 54
 Braun, R., & Walterbos, R. A. M. 1989, in *The Interstellar Medium in External Galaxies*, ed. D. Hollenbach & H. Thronson (NASA CP-3084), 269
 Brinks, E., & Shane, W. W. 1984, *A&AS*, 55, 179
 Burton, W. B. 1970, *A&AS*, 2, 261
 Bystedt, J. E. V., Brinks, E., De Bruyn, A. G., Israel, F. P., Schwering, P. B. W., Shane, W. W., & Walterbos, R. A. M. 1984, *A&AS*, 56, 245
 Colgan, S. W. J., Salpeter, E. E., & Terzian, Y. 1988, *ApJ*, 328, 275 (CST88)
 Colomb, F. R., Poppel, W. G. L., & Heiles, C. 1980, *A&AS*, 40, 47
 Cram, T. R., Roberts, M. S., & Whitehurst, R. N. 1980, *A&AS*, 40, 215
 Crovisier, J. 1981, *A&AS*, 94, 162
 Dickey, J. M. 1986, *ApJ*, 300, 190
 ———. 1990, in *Radio Observations of Nearby Spiral Galaxies*, ed. N. Duric (PASP Conf. Ser.), in press
 Dickey, J. M., & Brinks, E. 1988, *MNRAS*, 233, 781
 Dickey, J. M., Kulkarni, S. R., Van Gorkom, J. H., & Heiles, C. E. 1983, *ApJS*, 53, 591
 Dickey, J. M., Salpeter, E. E., & Terzian, Y. 1978, *ApJS*, 36, 77 (DST78)
 Dopita, M. A., Binette, L., D'Odorico, S., & Benvenuti, P. 1984, *ApJ*, 276, 653
 Draine, B. T. 1978, *ApJS*, 36, 595
 Garwood, R. W., & Dickey, J. M. 1989, *ApJ*, 338, 841
 Hagen, J. P., Lilly, A. E., & McClain, E. F. 1955, *ApJ*, 122, 365
 Henderson, A. P., Jackson, P. D., & Kerr, F. J. 1982, *ApJ*, 263, 116
 Kulkarni, S. R., & Heiles, C. 1988, in *Galactic and Extragalactic Radio Astronomy*, ed. K. I. Kellermann & G. L. Verschuur (Heidelberg: Springer-Verlag), 95
 Lazareff, B. 1975, *A&A*, 42, 25
 Lepp, S., & Dalgarno, A. 1988, *ApJ*, 335, 769
 Liszt, H. A. 1983, *ApJ*, 275, 163
 Lockman, F. J., Hobbs, L. M., & Shull, J. M. 1986, *ApJ*, 301, 380
 Mathis, J. S. 1983, *ApJ*, 267, 119
 Mebold, U. 1972, *A&A*, 19, 3
 Osterbrock, D. E. 1974, *Astrophysics of Gaseous Nebulae* (New York: Freeman), 66
 Payne, H. E., Salpeter, E. E., & Terzian, Y. 1982, *ApJS*, 48, 199 (PST82)
 ———. 1983, *ApJ*, 272, 540
 Peimbert, M. 1967, *ApJ*, 150, 825
 Pellet, A., Astier, N., Viale, A., Courtes, G., Maucherat, A., Monnet, G., & Simien, F. 1978, *A&AS*, 31, 439
 Press, W. H., Flannery, B. P., Teukolsky, S. A., & Vetterling, W. T. 1988, *Numerical Recipes* (Cambridge: Cambridge Univ. Press), 523
 Raymond, J. C. 1979, *ApJS*, 39, 1
 Savage, B. D., & Mathis, J. S. 1979, *ARA&A*, 17, 73
 Schmidt, M. 1957, *Bull. Astron. Inst. Netherlands*, 13, 247
 Talent, D. L., & Dufour, R. J. 1979, *ApJ*, 233, 888
 Unwin, S. C. 1980, *MNRAS*, 192, 259
 van Gorkom, J. H., Knapp, G. R., Ekers, R. D., Ekers, D. D., Laing, R. A., & Polk, K. S. 1989, *AJ*, 97, 708
 Walterbos, R. A. M., & Braun, R. 1989, in *The Interstellar Medium in External Galaxies*, ed. D. Hollenbach & H. Thronson (NASA CP-3084), 224
 ———. 1991, *A&AS*, in press
 Walterbos, R. A. M., & Kennicutt, R. C. 1988, *A&A*, 198, 61
 Walterbos, R. A. M., & Schwering, P. B. W. 1987, *A&A*, 180, 27